An explicit residual based approach for shallow water flows

Mario Ricchiuto

An explicit residual based approach for shallow water flows

M. Ricchiuto

RESEARCH REPORT

N° 8350

September 2013

Project-Team BACCHUS

ISSN 0249-6399 ISRN INRIA/RR--8350--FR+ENG

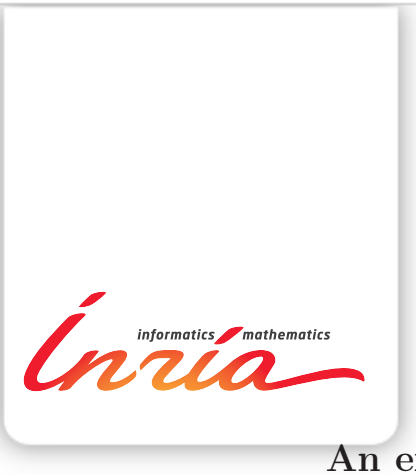

An explicit residual based approach for shallow water flows

M. Ricchiuto*

Project-Team BACCHUS

Research Report n° 8350 — September 2013 — 49 pages

Abstract: We describe a fully explicit residual based construction to discretize the shallow water equations with friction on unstructured grids. The approach is by construction exactly well balanced for al the simple known steady equilibria, and it shows a super-covergent behavior for smooth non-trivial equilibria, as the implicit residual schemes considered in (Ricchiuto, J.Sci.Comp. 48,2011). Moreover, by adapting the wetting drying technique discussed in (Ricchiuto and Bollermann, JCP 228, 2009) the scheme is able to preserve the non-negativity of the depth and to handle very well the runup and flooding of complex bathymetries. The approach is analyzed and tested thoroughly. The numerical results on a large variety of problems show the interest in the approach.

Key-words: free surface flow, shallow water equations, residual approach, residual distribution, explicit scheme, rung kutta scheme, unstructured grids, second order of accuracy, C-property, generalized C-property, positivity preservation, wetting-drying

* INRIA Bordeaux Sud-Ouest, 200 avenue de la Vieille Tour, 33405 Talence Cedex, France - mario.ricchiuto@inria.fr

RESEARCH CENTRE BORDEAUX – SUD-OUEST

351, Cours de la Libération
Bâtiment A 29
33405 Talence Cedex

An explicit residual based approach for shallow water flows

Résumé : On considère une construction explicite et residual based pour la discrétisation des équations shallow water sur maillages non-structurés. L'approche est par construction exactement well balanced pour tous les équilibres plus simples connus en littérature, mais il montre une super-convergence pour certains équilibres non-triviaux, comme les schémas implicites considérés en (Ricchiuto, J.Sci.Comp. 48,2011). En adaptant la stratégie de wetting/drying prsentée en (Ricchiuto and Bolermann, JCP 228, 2009) le schéma permet en plus de garantir la non-ngativité de la profondeur et de simuler runup et inondation de bathymétries complexes. La méthode est analysée et testée sur un nombre important de problèmes. Les résultats montrent l'intéret de l'approche

Mots-clés : free surface flow, shallow water equations, residual approach, residual distribution, explicit scheme, rung kutta scheme, unstructured grids, second order of accuracy, C-property, generalized C-property, positivity preservation, wetting-drying

Contents

1 Introduction

Free surface flows are relevant in a large number of applications, especially in civil and coastal engineering. The problems concerned and either (relatively) local, such as dam breaks and flooding, overland flows due to rainfall, nearshore wave propagation and interaction with complex bathymetries/structures, and tidal waves in rivers, or global such as in ocean or sea basin models for the

study of *e.g.* tsunami generation and propagation.

The simulation of such flows can be carried by solving directly the three dimensional Navier-Stokes equations. However, for many applications, including e.g. nearshore wave propagation and flooding, simplified models obtained by combining vertical averaging and some form of thin layer approximation provide reliable results. The applicability of such models depends on the nature of the flow and on the hypotheses at their basis [41, 12].

The simplest among these models is the so-called Shallow Water model. The model assumes that the waves developing in the flow are *long* (small ratio amplitude/wavelength), and of a hydrostatic vertical variation of the pressure [32, 44] . More complex nonlinear models can be obtained, by including higher order terms, and depending on the hypotheses on the flow [32, 44, 41, 12]. The first order shallow water approximation gives constitute a non-homogeneous hyperbolic system where the effects of the variation of the bathymetry and the viscous friction on the bottom are modeled by the source terms [32, 44].

The amount of literature related to the solution of the shallow water system is extremely vast. This model finds applications in oceanography, hydrology, and meteorology (see *e.g.* [69, 37, 17, 31, 70, 71] and references therein). The main challenges when solving the shallow water system numerically are related to the discretization of the bathymetry and friction terms, and to the numerical treatment of nearly dry regions. For the first issue, one speaks often *asymptotic preserving* character or *well balancedness* of a discretization. The second issue is what is referred to as the wetting/drying strategy.

Well balancing, refers to the ability of the discretization to preserve some steady equilibria involving the existence of a set of invariants exactly, or within some mesh size dependent bounds possibly more favorable than the accuracy of the scheme. The typical example is the so called *lake at rest state* involving a flat still free surface, that should be remaining flat whatever the shape of the bottom. This property is what one refers to as *Conservation property, or C-property* [11] or well-balancedness [33]. One speaks of approximate C-property when the steady state is kept within an accuracy higher than that of the underlying scheme. This property becomes important when one is interested in flows that, at least locally, are perturbation of one of these steady equilibria, so that numerical perturbations might interfere with the actual flow giving wrong results. There is plenty of literature discussing several different approaches to the preservation of steady equilibria, in particular the so-called lake at rest state. Most of these developments have taken place in the Finite Volume community, and are thought in terms of one-dimensional flows (see *e.g.* [11, 33, 30, 47] and references therein). The basic approach boils down either to the inclusion of a source term contribution in the FV numerical flux, so that the correct equilibrium is found at the discrete level [11, 33, 38], or to the rewriting of the system in a relaxation form, were an appropriate integral of the source term is added to the physical flux in the Maxwellian on the right hand side [26, 66] The extension to multiple space dimension is often done in a dimension by dimension basis on structured grids (see [79, 48, 47, 46], for recent examples), or introducing local one dimensional problems along some geometrical directions (*e.g.* normals to grid faces) [38, 25, 45, 9]. These modified FV fluxes are also used in the context of discontinuous Galerkin schemes to retain the C-property (see *e.g.* [77, 29]). Exceptions to this rule are the wave propagation scheme of LeVeque [42], continuous finite elements discretizations as the least squares Galerkin approach of G.Hauke [35], and Residual Distribution schemes [14, 54, 56].

Concerning the computational treatment of nearly dry areas involves the solution of the following issues : ensuring that in these regions no unphysical negative depths are obtained ; handling some ill-posed problems such as the computation of the local velocity given depth , and the discharge ;

preserving the well balanced character of the method when $0 < H \ll 1$.

These three issues are not independent and the large majority of the wetting/drying treatments discussed in literature boil down to : rely on the use of some positivity preserving scheme to be able to keep the depth non-negative ; introducing a cut-off of some sort on the velocity (and mass flux) to avoid zero over zero type divisions ; modify the *numerical* slope of the bathymetry used in the discrete equations ; employ an implicit (split or unsplit) treatment of the friction term to handle the stiffness associated to this term in dry areas. These ideas can be put in practice in various ways, depending on the initial formulation of the method, on the techniques used to reach higher order of accuracy, and on the type of nonlinear mechanism used to combine high order and preservation of the positivity. For an overview see [16, 15, 18, 19, 9, 29, 45, 80, 78].

In this paper, following the author's previous work [54, 56, 55] on the construction of residual approximations to the shallow water system, and the more recent work on the construction of genuinely explicit residual schemes [53, 50], we discuss the construction of a simple genuinely explicit residual based scheme allowing an efficient discretization of the shallow water equations with friction on unstructured meshes. The discussion is organized as follows. We recall the form of the shallow system and a number of exact steady equilibria in section §2. The explicit residual discretization approach is then recalled in section §3. Section §4 finally analyzes the properties of the discretization, namely well balancedness (C-properties), accuracy, positivity preservation, and wetting/drying strategy. Lastly, in section §5 we demonstrate the capabilities of the scheme on a large number of numerical tests. Conclusive remarks and future developments end the paper in section §6.

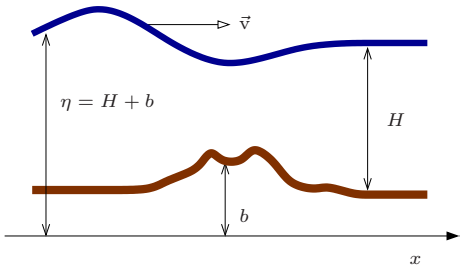

Figure 1: NLSW basic notation

2 The shallow water equations

The system of the Nonlinear Shallow Water Equations (NLSW) reads

$$\begin{aligned} \partial_t H + \nabla \cdot (H\vec{v}) + R(x,y,t) &= 0 \\ \partial_t (H\vec{v}) + \nabla \cdot (H\vec{v} \otimes \vec{v} + p(H)\mathbf{I}) + gH(\nabla b + c_f \vec{v}) &= 0 \end{aligned} \tag{1}$$

where (cf. figure 1) H represents the water depth, $\vec{v}$ the (vertically averaged) local velocity, R is a source of mass (*e.g.* associated to rainfall), b is the bathymetry, $p(h)$ is given by

$$p(H) = g\frac{H^2}{2}$$

and c_f is the friction coefficient generally depending on the solution :

$$c_f = c_f(h, \vec{v}) \tag{2}$$

In the following, we will assume that $R = 0$, and that the friction coefficient is given by Manning's formula

$$c_{\rm f} = \frac{n^2 \|\vec{\rm v}\|}{H^{4/3}} \tag{3}$$

with n the Manning's coefficient. Introducing the conserved variables u, conservative fluxes $\boldsymbol{\mathcal{F}}(u)$ and the source term $\boldsymbol{\mathcal{S}}$

$$u = \left[\begin{array}{c} H \\ H\vec{\rm v} \end{array} \right], \quad \boldsymbol{\mathcal{F}}(u) = \left[\begin{array}{c} H\vec{\rm v} \\ H\vec{\rm v} \otimes v + p(H)\mathbf{I} \end{array} \right], \boldsymbol{\mathcal{S}}(u,x,y) = gH \left[\begin{array}{c} 0 \\ \nabla b(x,y) + c_f(u)\vec{\rm v} \end{array} \right] \tag{4}$$

system (1) can be recast in the compact form

$$\partial_t u + \nabla \cdot \boldsymbol{\mathcal{F}}(u) + \boldsymbol{\mathcal{S}}(u,x,y) = 0 \tag{5}$$

System (1) is endowed with a mathematical entropy coinciding with the total energy [72, 74, 35, 36], it is hyperbolic, and characterized by the physical constraint of the non-negativity of the depth. Given a direction $\widehat{\xi} \in \mathbb{R}^2$, with $\|\widehat{\xi}\| = 1$, and setting for any $\vec{\rm v} \in \mathbb{R}^2$

$$\mathrm{v}_\xi = \vec{\rm v} \cdot \widehat{\xi} \tag{6}$$

the Jacobian matrix

$$\mathrm{K}_\xi = \frac{\partial \boldsymbol{\mathcal{F}}_\xi(u)}{\partial u} \tag{7}$$

admits a complete set of real eigenvalues and linearly independent real eigenvectors, with the eigenvalues given by

$$v_\xi - c\,, \quad v_\xi\,, \quad v_\xi + c$$

with c the celerity

$$c = \sqrt{gH} \tag{8}$$

It is also useful to introduce the free surface level

$$\eta = H + b\,, \tag{9}$$

the *specific total energy*

$$\mathcal{E} = g\eta + \mathrm{k}\,, \quad \mathrm{k} = \frac{\|\vec{\rm v}\|^2}{2}\,, \tag{10}$$

with k the kinetic energy, the discharge

$$\vec{q} = H\vec{\rm v}\,, \tag{11}$$

and the Froude number

$$\mathrm{Fr} = \frac{\|\vec{\rm v}\|}{c} \tag{12}$$

playing for (1) the same role as the Mach number in gas dynamics.

System (5) is known to admit a certain number of exact steady solutions whose form depend on the equilibrium between the source term $\boldsymbol{\mathcal{S}}$ and the remaining terms of the equation. In the following sub-sections we recall some of these solutions which will be used later to test the scheme.

2.1 Lake at rest solution

This solution corresponds to the hydrostatic equilibrium

$$\begin{aligned}\vec{q} =&0\\ \nabla p(H)+&gH\nabla b = 0\end{aligned}$$

The last relation is always satisfied by the physical steady state (cf. equation (9))

$$\begin{aligned}\vec{\mathrm{v}} =&0\\ \eta =&\eta_0 = \text{const}\end{aligned} \tag{13}$$

corresponding to still water on an arbitrary bathymetry.

2.2 Constant energy pseudo-1d flows

A pseudo one-dimensional steady equilibrium is readily obtained in the frictionless case by rewriting (1) as (cf. equation (10))

$$\begin{aligned}&\partial_t H + \nabla\cdot\vec{q} = 0\\ &\partial_t\vec{q} + (\vec{\mathrm{v}}\cdot\nabla)\,\vec{q} - \left(\vec{\mathrm{v}}^{\perp}\cdot\nabla\right)\vec{q}^{\perp} + \frac{1}{1-\mathrm{Fr}^2}\frac{1}{g}\left(gH\nabla\mathcal{E} - \vec{\mathrm{v}}\vec{\mathrm{v}}\cdot\nabla\mathcal{E}\right)\\ &\qquad + \frac{1}{1-\mathrm{Fr}^2}\left(\frac{\vec{\mathrm{v}}}{gH}\vec{\mathrm{v}}\cdot(\nabla\vec{q}\cdot\vec{\mathrm{v}}) - \mathrm{Fr}^2\left(\nabla\vec{q}\right)^t\cdot\vec{\mathrm{v}}\right) = \frac{\vec{\mathrm{v}}^{\perp}\cdot\nabla b}{1-\mathrm{Fr}^2}\vec{\mathrm{v}}^{\perp}\end{aligned} \tag{14}$$

with $\vec{\mathrm{v}}^{\perp} = (-\mathrm{v}_y, \mathrm{v}_x)$, $\vec{q}^{\perp} = H\vec{\mathrm{v}}^{\perp}$. Last equations show that indeed there exist an admissible family of steady solutions characterized by the invariants

$$\begin{aligned}\vec{q} =&\vec{q}_0 = \text{const}\\ \mathcal{E} =&\mathcal{E}_0 = \text{const}\end{aligned} \tag{15}$$

Note however that these solutions are constrained by the compatibility condition for the bathymetry

$$\vec{\mathrm{v}}^{\perp}\cdot\nabla b = 0 \tag{16}$$

allowing bathymetry variations only in the direction of the discharge. This makes these solutions basically one-dimensional flows in the $\vec{\mathrm{v}}$ direction.

2.3 Steady flows in sloping channels

If the bathymetry has a constant slope, a steady solution is obtained from the equilibrium between friction and the hydrostatic load. If we take

$$b = b_0 - \zeta_0 x$$

with constant slope ζ_0, and assume $\mathrm{v}_y = 0$ the equations reduce to

$$\begin{aligned}q_x &= q_0(y)\\ \partial_x H + c_{\mathrm{f}}(H,\vec{\mathrm{v}})\mathrm{v}_x &= \zeta_0\\ q_y &= 0\\ \partial_y\eta &= 0\end{aligned} \tag{17}$$

A known solution is given by the pseudo one-dimensional state

$$\begin{aligned} H =& H_0 = \text{const} \\ \mathrm{v}_x =& \mathrm{v}_0 = \text{const} \\ \mathrm{v}_y =& 0 \end{aligned} \tag{18}$$

When using Manning's formula (3), the values of H_0 and v_0 can be expressed as a function of the mass flux q_0 and of the slope as

$$\begin{aligned} H = H_0 &= \left(\frac{n^2 \|\vec{q}_0\|^2}{|\zeta_0|} \right)^{\frac{3}{10}} \\ \vec{\mathrm{v}} = \vec{\mathrm{v}}_0 &= - \left(\frac{|\zeta_0| \|\vec{q}_0\|^{4/3}}{n^2} \right)^{\frac{3}{10}} \frac{\nabla b}{|\zeta_0|} \end{aligned} \tag{19}$$

representing a pseudo one-dimensional flow in the direction of ∇b.

3 Explicit RK residual discretizations for conservation laws

3.1 Generalities

In this section we recall of the explicit residual schemes initially proposed in [53, 50]. Let us first recall that the NLSW can be recast in compact form as the system of nonlinear partial differential equations

$$\partial_t u + \nabla \cdot \boldsymbol{\mathcal{F}}(u) + \boldsymbol{\mathcal{S}}(u, x, y) = 0 \tag{20}$$

defined on a space-time domain $\Omega \times [0, T]$. We consider now an unstructured triangulation of Ω, which we denote by Ω_h, h denoting the largest element diameter. We denote by K the generic element of the mesh, and by $|K|$ its area. On Ω_h, we consider the standard continuous P^1 finite element approximation of u, which we denote by u_h. For every node $i \in \Omega_h$ we define K_i, the subset of elements containing i as a node

$$K_i = \bigcup_{K \in \Omega_h | i \in K} K \tag{21}$$

We denote by C_i the standard median dual cell obtained by joining the gravity centers of the elements in K_i with the mid-points of the edges emanating from i whose area is given by

$$|C_i| = \sum_{K \in K_i} \frac{|K|}{3} \tag{22}$$

The temporal domain $[0, T]$ is approximated by a set of time slabs $[t^n, t^{n+1}]$. We denote by $\Delta t^n = t^{n+1} - t^n$, and we set $\Delta t = \max_n \Delta t^n$.

As summarized on figure 2, the approach proposed follows the Residual Distribution (RD) philosophy inspired by the fluctuation and signals framework initially introduced by P.L. Roe [61]. According to this principle, data are evolved by means of signals proportional to a local error in the approximation of the equation (Roe's fluctuation).

This framework has led to the development of a certain number of numerical schemes known as the fluctuation splitting, or more recently, Residual Distribution schemes. For a review, the interested reader can consult [2, 3, 24, 62] and references therein. For the time dependent NLSW, the most recent adaptation of this approach is discussed in [56, 55]. The scheme proposed in the

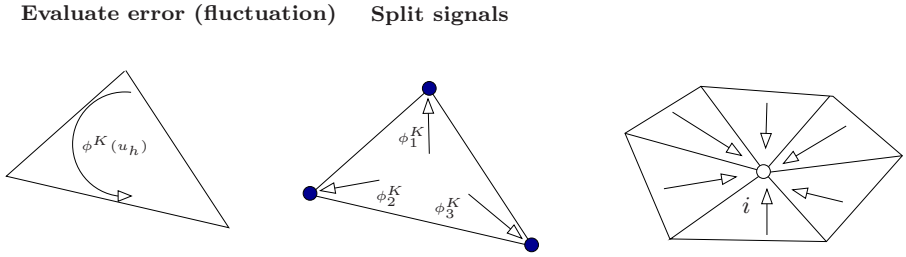

Figure 2: Residual Distribution/Fluctuation splitting methodology

last references allows to solve the NLSW with second order of accuracy for smooth solutions on unstructured grids, it satisfies the C-property [11] for the lake at rest state, and an approximate generalized C-property for the pseudo one-dimensional flow of section §2.2 [52], it preserves the positivity of the depth, and, in conjunction with a proper wetting and drying strategy, allows the approximation of solutions involving runup, drying and flooding of complex bathymetries.

The main flaw of the scheme of [56, 55] is that, even though the scheme is highly implicit, positivity preservation is only achieved under an explicit time step restriction dictated by the underlying Crank-Nicholson time integration. In order to overcome this limitations, two strategies have been proposed. One is the genuinely space-time formulation of [39], extended to the NLSW in [64]. The second is the genuinely explicit Runge-Kutta predictor-corrector variant of [53, 50]. Preliminary results on the application of the latter to the NLSW have been presented in [50, 51]. Here we will analyze and extend the study of the last reference.

3.2 The predictor-corrector explicit scheme

Given the approximation of the initial solution u_h^0, in its simplest form, the scheme of [53, 50, 51] applied to the NLSW allows to march in time according to the following computational procedure :

1. Predictor step :

   - $\forall\, K \in \Omega_h$ compute the *fluctuation* defined as

   $$\phi^K(u_h^n) = \oint_{\partial_K} \boldsymbol{\mathcal{F}}_h(u_h^n)\cdot\hat{n} + \int_K \boldsymbol{\mathcal{S}}_h(u_h^n, x, y) \tag{23}$$

   - $\forall\, K \in \Omega_h$ distribute the *fluctuation* to the nodes of K. If ϕ_i^K denotes the amount of ϕ^K distributed to node $i \in K$, then

   $$\sum_{j\in K} \phi_j^K(u_h^n) = \phi^K(u_h^n) \tag{24}$$

   Equivalently, if there exist *bounded distribution matrix coefficients* β_i^K such that

   $$\phi_i^K = \beta_i^K \phi^K \tag{25}$$

   then the *consistency condition* (24) becomes

   $$\sum_{j\in K} \beta_j^K = \mathbf{I} \tag{26}$$

- $\forall\, i \in \Omega_h$ compute the first order predictor u_i^* from

$$|C_i|\frac{u_i^* - u_i^n}{\Delta t^n} + \sum_{K \in K_i} \phi_i^K(u_h^n) = 0 \tag{27}$$

2. Corrector step :

- $\forall\, K \in \Omega_h$ compute the *element residual* defined as (cf. equation (23))

$$\Phi^K(u_h^n, u_h^*) = \int_K \frac{u_h^* - u_h^n}{\Delta t^n} + \frac{1}{2}\phi^K(u_h^n) + \frac{1}{2}\phi^K(u_h^*) \tag{28}$$

  Note that, as in [53], we distinguish between the fluctuation (23), containing the integral of the spatial operator, and the element residual (28), defined as the integral of the full semi-discrete equation.

- $\forall\, K \in \Omega_h$ distribute the *element residual* to the nodes of K. If Φ_i^K denotes the amount of Φ^K distributed to node $i \in K$, then

$$\sum_{j \in K} \Phi_j^K(u_h^n, u_h^*) = \Phi^K(u_h^n, u_h^*) \tag{29}$$

  As before, if there exist *bounded distribution matrix coefficients* β_i^K such that

$$\Phi_i^K = \beta_i^K \Phi^K \tag{30}$$

  then the distribution matrices must verify the consistency condition (26)

- $\forall\, i \in \Omega_h$ compute the second order correction from

$$|C_i|\frac{u_i^{n+1} - u_i^*}{\Delta t^n} + \sum_{K \in K_i} \Phi_i^K(u_h^n, u_h^*) = 0 \tag{31}$$

In the above expressions it remains to specify not only how the distribution is performed, but also how to define the *discrete approximation of the flux and of the source term* $\boldsymbol{\mathcal{F}}_h(u_h)$, and $\boldsymbol{\mathcal{S}}_h(u_h, x, y)$, given the nodal values of the solution.

Remark 3.1 (Fluctuation and signals)**.** *With the notation introduced so far, we can easily recall that the implicit scheme of [56, 55] can be recast as : given the initial solution* u_h^0 *march in time by solving the nonlinear sistem*

$$\sum_{K \in K_i} \Phi_i^K(u_h^n, u_h^{n+1}) = 0\,, \quad \forall\, i \in \Omega_h$$

where $\forall\, K \in \Omega_h$ *the quantity* $\Phi_i^K(u_h^n, u_h^{n+1})$ *is a splitting of the element residual*

$$\Phi^K(u_h^n, u_h^{n+1}) = \int_K \frac{u_h^{n+1} - u_h^n}{\Delta t^n} + \frac{1}{2}\phi^K(u_h^n) + \frac{1}{2}\phi^K(u_h^{n+1}) = \sum_{j \in K} \Phi_j^K(u_h^n, u_h^{n+1})$$

It is immediately clear that the scheme of [56, 55] would be, eventually, obtained using (31) *as an iterative scheme to get to the fixed point* $u_i^* = u_i^{n+1}$.

The right hand sides of (27) *and* (31) *are thus easily interpreted as corrections of the nodal values somehow proportional to elemental errors given by the integral of the equations, represented by the residual* Φ^K. *This allows to view the scheme proposed as a truly time dependent generalization of Roe's initial fluctuation splitting idea [61].*

3.3 Basic properties

The basic properties of the explicit scheme described in the previous section are thoroughly discussed in [53, 50]. We recall here the conditions under which scheme (23)-(31) is conservative, second order accurate, and satisfies a discrete maximum principle.

Conservation. By conservation we mean the ability to reproduce the correct jump conditions across discontinuous solutions. This property is characterized by a Lax-Wendroff theorem firstly formulated in [5], and then further clarified in [4, 7] and in [23, 58]. Without going into the details of the theorem, for which we refer the reader to [5, 4, 7], we recall that *provided that the consistency conditions* (24) *and* (29) *hold, scheme* (23)-(31) *is conservative if the discrete approximation of the physical flux* $\boldsymbol{\mathcal{F}}_h(u_h)$ *is continuous across edges.*

Note that this continuity condition is satisfied by several definitions of the discrete flux, such as $\boldsymbol{\mathcal{F}}_h(u_h) = \boldsymbol{\mathcal{F}}_h$ the P^1 finite element interpolation of the nodal values of the flux, or also $\boldsymbol{\mathcal{F}}_h(u_h) = \boldsymbol{\mathcal{F}}(u_h)$, and more generally by $\boldsymbol{\mathcal{F}}_h(u_h) = \boldsymbol{\mathcal{F}}(u(v_h))$ where v_h is the finite element interpolation of a set of variables different from u. A similar set of choices is possible for $\boldsymbol{\mathcal{S}}_h(u_h, x, y)$ as well. This freedom can be exploited to recognize steady equilibria, as we shall see later.

Second-order. As discussed in much detail in [53, 50], scheme (23)-(31) can obtained as a particular case of a mass lumped P^1 Petrov-Galerkin finite element discretization. In particular, in order to formally characterize the accuracy, let us consider a smooth exact pointwise solution $w(x, y, t)$, such that

$$\partial_t w + \nabla \cdot \boldsymbol{\mathcal{F}}(w) + \boldsymbol{\mathcal{S}}(w, x, y) = 0 \quad \forall (x, y, t) \in \Omega \times [0,\, T]$$

Let w_i^n be its nodal values at the discrete time level t^n, and w_h^n the finite element approximation at the same time level. Consider also a C^1 continuous compactly supported function $\psi \in C_0^1(\Omega \times [0,\, T])$, and define the truncation error

$$\epsilon := \sum_{n=1}^{N} \sum_{i \in \Omega_h} \psi_i^n \left[|C_i| \frac{w_i^{n+1} - w_i^*}{\Delta t^n} + \sum_{K \in K_i} \Phi_i^K(w_h^n, w_h^*) \right] \tag{32}$$

with $\sum_{n=1}^{N} \Delta t^n = T$, and w_i^* obtained from (27) :

$$|C_i| \frac{w_i^* - w_i^n}{\Delta t^n} + \sum_{K \in K_i} \phi_i^K(w_h^n) = 0 \tag{33}$$

In [53, 50] it is proven that *if there exist distribution matrix coefficients* $\{\beta_j^K\}_{j \in K}$ *uniformly bounded w.r.t.* h, w_h, ϕ^K, Φ^K *and the data of the problem, such that* (25) *and* (30) *hold, then*

$$\begin{aligned}
&\epsilon + \mathcal{O}(\Delta t^2) = \\
&\int_0^T \int_{\Omega_h} \psi_h \partial_t (w_h - w) + \int_0^T \int_{\Omega_h} (\boldsymbol{\mathcal{F}}(w) - \boldsymbol{\mathcal{F}}_h(w_h)) \cdot \nabla \psi_h + \int_0^T \int_{\Omega_h} (\boldsymbol{\mathcal{S}}_h(w_h, x, y) - \boldsymbol{\mathcal{S}}(w, x, y)) \psi_h \\
&+ \sum_{n=1}^{N} \sum_{K \in \Omega_h} \sum_{i,j \in K} \Delta t^n \frac{\psi_i^n - \psi_j^n}{3} \int_K \gamma_i^K \left(\partial_t (w_h - w) + \nabla \cdot (\boldsymbol{\mathcal{F}}_h(w_h) - \boldsymbol{\mathcal{F}}(w)) + \boldsymbol{\mathcal{S}}_h(w_h, x, y) - \boldsymbol{\mathcal{S}}(w, x, y) \right)
\end{aligned}$$

with γ_i^K *a suitably chosen uniformly bounded Petrov-Galerkin bubble stabilization depending on the distribution coefficients* β_i^K*. Moreover, under the same hypotheses, and provided that there exist*

positive bounded constants C_1, C_2, C_a, C_b *such that*

$$C_1 \leq \max_{K\in\Omega_h} \frac{h^2}{|K|} \leq C_2 \qquad C_a \leq \frac{\Delta t}{h} \leq C_b \tag{34}$$

then the error can be bounded using classical approximation arguments to obtain the consistency estimate :

$$|\epsilon| \leq C(\Omega_h, T, \psi)h^2 \tag{35}$$

For further details, the interested reader can consult [53, 50]. We limit ourselves to observe that the key to second order of accuracy is the uniform boundedness of the distribution coefficients (25), (30).

Discrete Maximum Principle. The non-oscillatory character of the discretization is preserved in the Residual Distribution framework by making use of the theory of positive coefficient schemes [68, 10, 24]. The theory mainly deals with the case in which (20) reduces to a scalar homogeneous conservation law

$$\partial_t u + \nabla \cdot \boldsymbol{\mathcal{F}}(u) = 0$$

In this case, scheme (23)-(31) remains formally identical, modulo the fact that $\boldsymbol{\mathcal{S}} = 0$. In summary, the idea is to ensure that in (27) and (31) one has $\forall\, K$

$$\phi_i^K = \sum_{j\in K} c_{ij}^n (u_i^n - u_j^n)\,, \;\; \Phi_i^K = \frac{1}{2}\sum_{j\in K} c_{ij}^* (u_i^* - u_j^*) + \frac{1}{2}\sum_{j\in K} \overline{c}_{ij}^n (u_i^n - u_j^n) \quad \text{with } c_{ij}^n,\, c_{ij}^*,\, \overline{c}_{ij}^n \geq 0 \tag{36}$$

Under this hypothesis one easily shows that under the time step restriction $\Delta t^n \leq |C_i| / \sum_K \sum_{j\in K} c_{ij}^n$ the predictor step verifies

$$\min_{j\in K_i} u_j^n \leq u_i^* \leq \max_{j\in K_i} u_j^n$$

For the corrector step we can write

$$\begin{aligned} u_i^{n+1} =& u_i^* - \frac{\Delta t^n}{2|C_i|} \sum_{K\in K_i}\sum_{j\in K} c_{ij}^* (u_i^* - u_j^*) - \frac{\Delta t^n}{2|C_i|} \sum_{K\in K_i}\sum_{j\in K} \overline{c}_{ij}^n (u_i^n - u_j^n) \\ =& \frac{1}{2}\left(u_i^* - \frac{\Delta t^n}{|C_i|} \sum_{K\in K_i}\sum_{j\in K} c_{ij}^* (u_i^* - u_j^*) \right) + \frac{1}{2}\left(u_i^n - \frac{\Delta t^n}{|C_i|} \sum_{K\in K_i}\sum_{j\in K} (\overline{c}_{ij}^n + c_{ij}^n)(u_i^n - u_j^n) \right) \end{aligned}$$

so, provided that

$$\Delta t^n \leq \min\left(\frac{|C_i|}{\sum\limits_{K\in K_i}\sum\limits_{j\in K} c_{ij}^*}, \frac{|C_i|}{\sum\limits_{K\in K_i}\sum\limits_{j\in K} (c_{ij}^n + \overline{c}_{ij}^n)}\right)$$

we have

$$\frac{1}{2}\min_{j\in K_i} u_j^* + \frac{1}{2}\min_{j\in K_i} u_j^n \leq u_i^{n+1} \leq \frac{1}{2}\max_{j\in K_i} u_j^* + \frac{1}{2}\max_{j\in K_i} u_j^n$$

For scalar homogeneous problems, the theory of positive coefficient schemes allows to give precise conditions leading to local bounds on the numerical solution, related to the local extrema at the of time level. For a hyperbolic system things become much more complicated, and even in the continuous case the existence of maximum principles is hard to prove in a general way, its definition being unclear even at the continuous level. We mention that a discrete wave decomposition technique has been proposed in [6] as a means to extend positive coefficient schemes theory to systems.

In this paper, we will say that *a scheme is positive if it verifies* (36) *in the scalar case.* For the NLSW (and for systems in general) practical tests show that indeed these schemes show a

non-oscillatory approximation of discontinuities. Using the same theory, however, in section §4 we shall study in more detail the preservation of the physical constraint $H \geq 0$ for the scheme used in all the numerical applications.

4 Application to the Shallow Water equations

We consider now the properties of scheme (23)-(31) when applied to the NLSW. Two issues are analyzed : the preservation of steady equilibria, and the wetting/drying strategy, including the issue of the preservation of the constraint $H \geq 0$. The analysis of the preservation of steady equilibria is general and applies to all schemes that formally verify (25) and (30). On the contrary, so far computations involving dry areas rely on nonlinear Lax-Friedrich's distribution initially introduced in [1], and constituting the basis of the results presented in [56, 55] for the NLSW.

4.1 C-property and super-consistency analysis

The C-property or "conservation" property, introduced in of [11], consists of the ability of the discretization in preserving the exact steady state balance of flux divergence and source terms. Originally, a scheme was said to enjoy the C-property if it preserved exactly the steady state (13). However one still speaks of C-property when referring to other steady states [20]. When the conservation of the steady state is no exact but is obtained within error rates below the formal accuracy of the scheme, one often speaks of generalized C-property [52]. Schemes enjoying the C-property, of the generalized C-property, are more often referred to in literature as being "well balanced". In this paper we will say that a scheme verifies the C-property for a given steady state, if that state is preserved exactly by the scheme. If the preservation is obtained within error bounds decreasing with rates larger than those of the formal accuracy of our scheme, we will speak of *super consistency* or *super convergence* for that particular solution.

For the schemes considered here, we start by providing a general result concerning smooth steady equilibria admitting a set of invariants. In the next section, we will analyze the case of the particular steady solutions discussed in section §2.

The underpinning idea is that if for a given state $u = u^0(x)$ we have $\phi^K(u^0) = 0$, then the scheme defined by (23)-(31), (25) and (30) will preserve the initial state indefinitely since

$$|C_i|\frac{u_i^* - u_i^0}{\Delta t^n} = |C_i|\frac{u_i^{n+1} - u_i^*}{\Delta t^n} = 0$$

The objective of the analysis is to quantify the effect of the approximation choice and of the quadrature errors in the evaluation of ϕ^K on the preservation of smooth equilibria.

To start, we assume here that *both the flux* $\boldsymbol{\mathcal{F}}$ *and the source term* $\boldsymbol{\mathcal{S}}$ *are at least Lipschitz continuous* :

$$\|\boldsymbol{\mathcal{F}}(u) - \boldsymbol{\mathcal{F}}(w)\| \leq \mathcal{K}_{\boldsymbol{\mathcal{F}}}\|u - w\| \quad \text{and} \quad \|\boldsymbol{\mathcal{S}}(u, \nabla b) - \boldsymbol{\mathcal{S}}(w, \nabla b)\| \leq \mathcal{K}_{\boldsymbol{\mathcal{S}}}\|u - w\| \tag{37}$$

Consider now a set of derived variables v that depend on u, and that also depend on b. In particular, we consider now the mappings

$$v \ : \ (u,\, b) \mapsto v(u, b)\,, \quad U = v^{-1} \ : (v,\, b) \mapsto u = U(v, b) \tag{38}$$

It is assumed in the following that these mappings are smooth. Examples of such variables are

- Total energy variables (cf. equation (10)) : $v = \left[\mathcal{E}\,, \vec{q}\right]^t$
- Symmetrizing variables [73, 75, 35, 36] : $v = \left[g\eta - \mathrm{k},\, \vec{\mathrm{v}}\right]^t$

The flux being independent on b, we can express the divergence term as (cf. equation (38))

$$\begin{aligned}\nabla \cdot \boldsymbol{\mathcal{F}}(u(v,b)) =& \frac{\partial \boldsymbol{\mathcal{F}}}{\partial u}(u(v,b))\frac{\partial u}{\partial v}(u(v,b)) \cdot \nabla v + \frac{\partial \boldsymbol{\mathcal{F}}}{\partial u}(u(v,b))\frac{\partial U}{\partial b}(u(v,b)) \cdot \nabla b \\ =& \frac{\partial \boldsymbol{\mathcal{F}}}{\partial v}(u(v,b)) \cdot \nabla v + \boldsymbol{\mathcal{S}}_v(u, \nabla b)\end{aligned} \tag{39}$$

where $\boldsymbol{\mathcal{S}}_v(u, \nabla b)$ is the contribution of all the terms containing derivatives of the bathymetry. For the analysis that follows we make the additional hypothesis of the explicit knowledge of an analytical bathymetry and of the definition of the continuous flux approximation and discrete source term built starting from the nodal values of the steady invariant, and from the local values of $b(x, y)$, namely

$$\boldsymbol{\mathcal{F}}_h = \boldsymbol{\mathcal{F}}(u(v_h, b))\,, \quad \boldsymbol{\mathcal{S}}_h = \boldsymbol{\mathcal{S}}(u(v_h, b), \nabla b) \tag{40}$$

Using this notation, we can prove the following result.

Lemma 4.1 (Super consistency - local estimate)**.** *Given an analytical bathymetry b, let $v(u, b)$ be a set of invariants such that a family of steady equilibria for* (1) *is completely described by*

$$v = v_0 = const$$

Let $\boldsymbol{\mathcal{F}}_h = \boldsymbol{\mathcal{F}}(u(v_h, b))$ and $\boldsymbol{\mathcal{S}}_h = \boldsymbol{\mathcal{S}}(u(v_h, b), \nabla b)$, with v_h the piecewise linear continuous P^1 approximation of v. Assume that $(v, b) \mapsto u$ is a one to one smooth mapping C^l with l sufficiently large, and similarly $(v, b) \mapsto \boldsymbol{\mathcal{F}}(u(v, b))$ is also $C^{l'}$ with l' sufficiently large. Then, for exact integration we have

$$\phi^K(v_0, b) = \oint_{\partial K} \boldsymbol{\mathcal{F}}_h \cdot \vec{n} + \int_K \boldsymbol{\mathcal{S}}_h = 0$$

For approximate integration, let

$$\phi^K(v_0, b) = \sum_{f \in \partial K} \sum_{q=1}^{f_q} \omega_q \boldsymbol{\mathcal{F}}_h(\vec{x}_q) \cdot \vec{n}_f + \sum_{q=1}^{v_q} \overline{\omega}_q \boldsymbol{\mathcal{S}}_h(\vec{x}_q)$$

and let the line quadrature formula used for the flux be exact for polynomials of degree $p_f \geq 1$, and the volume quadrature formula used for the source be exact for polynomials of degree $p_v \geq 1$. If $b \in H^{p+1}(\Omega)$ with $\nabla b \in H^p(\Omega_h)$ and with $p \geq \min(p_f,\, p_v + 1)$, then

$$|\phi^K(v_0, b)| \leq C\, h^r \quad \textit{with} \quad r = \min(p_f + 2,\, p_v + 3)$$

Proof. See appendix A. □

The meaning of the last proposition is the following : *for a smooth enough bathymetry, provided that the approximation is written in terms of the steady invariants, the fluctuation* (23) *is small, and its magnitude is dictated by the numerical quadrature used in practice.*

Under the same hypotheses and with the same notation of the lemma, in appendix A we prove the following more general result.

Proposition 4.2 (Super consistency)**.** *Under the regularity assumptions on the mesh and on the time step* (34)*, and provided that* (25)-(30) *are true for some distribution coefficients* β_i^K *uniformly bounded w.r.t.* h*,* u_h*, element residuals, and w.r.t. to the data of the problem, then scheme* (23)-(31) *preserves exactly the initial steady equilibrium for exact integration. For approximate integration, under the same hypotheses of lemma 4.1 scheme* (23)-(31) *verifies a the truncation error estimate*

$$|\epsilon(v_0, b, \psi)| \leq C\, h^l\,, \quad l = \min(p_f + 1,\, p_v + 2) \tag{41}$$

with the error $\epsilon(v_0, b, \psi)$ *defined as in* (32)*.*

Some remarks are in order. The last proposition shows that for finite time computations, if the bathymetry is regular enough, the discrete solution converges with a rate $l > 2$, as soon as the quadrature formulae are more than second order accurate. The proposition explicitly uses the assumption that an analytical bathymetry is used in the discretization, and that the regularity of this expression is such that the full accuracy of the quadrature formulas is recovered. As the numerical examples will show, in practice the convergence rates saturate at a value that depends on the regularity of the bathymetry as

$$\epsilon(v_0, b, \psi) = \mathcal{O}(h^l)\,, \quad l = \min(p + 1, p_f + 1, p_v + 2) \tag{42}$$

with $b \in H^{p+1}(\Omega)$. As we will see, this implies that for piecewise continuous bathymetries with locally discontinuous slopes, only first order of accuracy is obtained when using for the flux the continuous approximation (40). In these cases, we will also show that a better result is obtained for the lake at rest solution when replacing $b(x, y)$ by its finite element approximation.

A similar but more general result involving other time discretization strategies is proved in [50], while numerical results confirming a similar behavior for the schemes of [56] have been already discussed in [52].

4.2 C-property : application to particular steady states

In this section we make a case by case analysis of the steady solutions presented in section §2. The principle used will be always to write the continuous approximation of the fluxes and the one of the source term starting from nodal values of the steady state in variants. The discussion made here will be confirmed by the numerical experiments of section §5. As in [11, 20] we will refer to the exact conservation of a steady equilibrium as to the C-property, while, following section §4.1, we will talk of super consistency when preservation is only obtained within an error below the theoretical truncation error of the schemes.

4.2.1 The lake at rest solution

The approximation of this solution by means of RD type discretization has been thoroughly studied in [14, 54, 56, 52]. We can distinguish two cases. The first is the one in which the approach of section §4.1 is used, and the discrete flux and source term approximations are written as (40). In this case,the discussion of the previous section leads to the result that follows.

Proposition 4.3 (Lake at rest - super consistency)**.** *Given an analytical bathymetry* b*, let* $v(u, b) = [\eta,\, \vec{q}]$*, with* η *the free surface level* (9)*, such that the lake at rest state is described by*

$$v = v_0 = [\eta_0,\, 0]$$

Let the discrete flux approximation be defined by (40) *with* v *given above Then, for exact integration scheme* (23)-(31) *preserves* exactly *the lake at rest state. For approximate integration, let the line quadrature formulas used in* (23) *be exact for polynomials of degree* $p_f \geq 1$*, and the volume quadrature formula be exact for polynomials of degree* $p_v \geq 1$*; if* $b \in H^{p+1}(\Omega)$ *with* $\nabla b \in H^p(\Omega_h)$*, and provided that* (25)-(30) *are true for some distribution coefficients* β_i^K *uniformly bounded w.r.t.* h*,* u_h*, element residuals, and w.r.t. to the data of the problem, then scheme* (23)-(31) *is super-consistent for the lake at rest state in the sense of the error estimate* (42)*.*

In this case, we note that the components of physical flux $\boldsymbol{\mathcal{F}}$ are polynomials of degree at most 3 of the components of v, so that accurate numerical quadrature becomes quite easy. However, for bathymetries with low regularity, this approach will yield errors of $\mathcal{O}(h)$ which is above the formal accuracy of the scheme, even for such a simple solution.

A more interesting approach is that used already in [14, 54, 56], consisting in replacing b by its finite element approximation. In this case, one simply finds that the discrete approximation of H obtained as $H_h = \eta_h - b_h$ is exactly that which would be obtained by approximating directly H. Moreover, following the above references, we can readily show that along the lake at rest state

$$\begin{aligned}\phi^K(v_0) &= \int_{\partial K} \begin{bmatrix} H_h\vec{\mathrm{v}}_h \\ H_h\vec{\mathrm{v}}_h \otimes \vec{\mathrm{v}}_h + g\frac{H_h^2}{2}\mathbf{I} \end{bmatrix} \cdot \vec{n} + \int_K gH_h \begin{bmatrix} 0 \\ \nabla b_h + c_{\mathrm{f}}\vec{\mathrm{v}}_h \end{bmatrix} \\ &= \int_{\partial K} \begin{bmatrix} 0 \\ g\frac{H_h^2}{2}\mathbf{I} \end{bmatrix} \cdot \vec{n} + \int_K gH_h \begin{bmatrix} 0 \\ \nabla b_h \end{bmatrix} = \int_K gH_h \begin{bmatrix} 0 \\ \nabla \eta_h \end{bmatrix} = 0\end{aligned}$$

where all the can be evaluated exactly by means of simple Gauss quadrature formulae. This leads to the following result.

Proposition 4.4 (Lake at rest - C-property)**.** *For a given bathymetry* $b(x, y)$ *let* b_h *be its finite element approximation. Let the discrete approximation of the flux be given by* $\boldsymbol{\mathcal{F}}_h = \boldsymbol{\mathcal{F}}([H_h, \vec{q}_h]^t)$*. Provided that the quadrature formulae used in* (23) *are exact w.r.t* H_h^2*, provided that* (25)-(30) *are true for some distribution coefficients* β_i^K *uniformly bounded w.r.t.* h*,* u_h*, element residuals, and w.r.t. to the data of the problem, then then scheme* (23)-(31) *preserves exactly the lake at rest solution, independently on the regularity of* $b(x, y)$*.*

4.2.2 Constant energy pseudo-1d flows

The constant energy pseudo-1d solution equilibrium fits quite well in the analysis made in section §4.1. Numerical results showing that a super convergent behavior is observed when interpolating directly the total energy have been already reported in [52] for the scheme of [56]. The analysis of section §4.1 proves the following.

Proposition 4.5 (Constant energy pseudo-1d flows - super consistency)**.** *Given an analytical bathymetry* b*, let* $v(u, b) = [\mathcal{E}, \vec{q}]$*, with* $\mathcal{E}$ *the total energy* (10) *and* $\vec{q}$ *the discharge* (11)*, such that the exact steady state is described by*

$$v = v_0 = [\mathcal{E}_0, \vec{q}_0]$$

Let the discrete flux approximation be defined by (40)*. Then, for exact integration scheme* (23)-(31) *preserves* exactly *constant energy pseudo-1d flow equilibria. For approximate integration, let the line quadrature formulas used in* (23) *be exact for polynomials of degree* $p_f \geq 1$*, and the volume quadrature formula be exact for polynomials of degree* $p_v \geq 1$*; if* $b \in H^{p+1}(\Omega)$ *with* $\nabla b \in H^p(\Omega_h)$*, and provided that* (25)-(30) *are true for some distribution coefficients* β_i^K *uniformly bounded w.r.t.*

h, u_h, element residuals, and w.r.t. to the data of the problem, then scheme (23)-(31) *is super-consistent for constant energy pseudo-1d flows in the sense of the error estimate* (42).

This result is similar to other results presented *e.g.* in [30, 47, 79]. However, as the numerical results will show, here we obtain a super convergent behavior on unstructured triangular meshes, while only one dimensional and two dimensional cartesian meshes have been studied previously, with the exception of the author's previous work [52].

As discussed in detail in [47], when writing the approximation in terms of the energy variables $[\mathcal{E}, \vec{q}]^t$, the local values of the set $[H, \vec{\mathrm{v}}]^t$ are obtained as the solution of a nonlinear algebraic problem. In particular, given a tuple $[\mathcal{E}^*, \vec{q}^*]$, and the local value of the bathymetry b^*, in order to obtain the corresponding values of H and $\vec{\mathrm{v}}$ needed to evaluate the flux, one needs to solve the nonlinear system (cf. equation (10))

$$
\begin{aligned}
&H\vec{\mathrm{v}} = \vec{q}^* \\
&gH + \frac{\vec{\mathrm{v}} \cdot \vec{\mathrm{v}}}{2} = \mathcal{E}^* - gb^*
\end{aligned}
$$

where, using the first equation one obtains a cubic algebraic equation for H :

$$
H^3 + \big(b^* - \frac{\mathcal{E}^*}{g}\big)H^2 + \frac{\vec{q}^* \cdot \vec{q}^*}{2g} = 0
$$

The conditions for the existence of solutions to this equation, and a small summary of the Newton algorithm necessary to obtain them, are given in [47] which we have followed in all the numerical applications discussed in section §5.

4.2.3 Steady flows in sloping channels

These solutions are a particularly simple example of steady equilibrium between friction and a constant slope. In this case, H, $\vec{\mathrm{v}}$, and $\vec{q}$ are constant. The friction term $c_{\mathrm{f}}(H_0, \vec{\mathrm{v}}_0)$ exactly balances the constant slope $\nabla b = \zeta_0$ (cf. section §2.3). Simple algebra shows that in this case approximating directly the conserved variables $[H, \vec{q}]^t$ leads to the identity

$$
\phi^K = \oint_{\partial K} \begin{bmatrix} \vec{q}_0 \\ \vec{q}_0 \otimes \vec{\mathrm{v}}_0 + g\frac{H_0^2}{2}\mathbf{I} \end{bmatrix} \cdot \vec{n} + \int_K gH_h \begin{bmatrix} 0 \\ \overbrace{\nabla b_0 + c_{\mathrm{f}}\vec{\mathrm{v}}_0}^{=0} \end{bmatrix} = \begin{bmatrix} \vec{q}_0 \\ \vec{q}_0 \otimes \vec{\mathrm{v}}_0 + g\frac{H_0^2}{2}\mathbf{I} \end{bmatrix} \cdot \overbrace{\oint_{\partial K} \vec{n}}^{=0} = 0
$$

This result is independent on how the integrals are evaluated, thus proving the following property.

Proposition 4.6 (Steady flows in sloping channels - C-property)**.** *Given the constant slope bathymetry $b(x) = b_0 - \zeta_0 x$, let the discrete approximation of the flux be given by $\boldsymbol{\mathcal{F}}_h = \boldsymbol{\mathcal{F}}([H_h, \vec{q}_h]^t)$. Provided that* (25)-(30) *are true for some distribution coefficients β_i^K uniformly bounded w.r.t. h, u_h, element residuals, and w.r.t. to the data of the problem, then scheme* (23)-(31) *preserves exactly steady flows on constant sloping channels, independently on the quadrature formulae used in* (23).

4.3 Nonlinear Lax-Friedrich's distribution

The super-convergence properties and the C-property discussed in the previous sections are independent on the actual form of the distribution coefficient, and are valid as long as this coefficient is bounded. To complete the presentation of the scheme used in the numerical validation we consider in this section the issue of the preservation of the depth non-negativity, and, in the following, that

of the treatment of wet-dry fronts.

The scheme used in this work is the nonlinear variant of the Lax-Friedrich's scheme in the stabilized form originally proposed in [1], and further adapted for the solution of the time dependent NLSW in [56, 55]. As in the references, the starting point of the construction is the first order Lax-Friedrich's distribution (cf. section §3.2 equations (23), (24), and (27))

$$\phi_i^{\rm LF}(u_h^n) = \frac{\phi^K(u_h^n)}{3} + \frac{\alpha_{\rm LF}}{3}\sum_{j\in K}(u_i^n - u_j^n) \tag{43}$$

in the predictor step and (cf. section §3.2 equations (28), (29), and (31))

$$\Phi_i^{\rm LF} = \frac{|K|}{3}(u_i^* - u_i^n) + \frac{\phi_i^{\rm LF}(u_h^n) + \phi_i^{\rm LF}(u_h^*)}{2} \tag{44}$$

in the corrector step. The usual definition of the LF dissipation coefficient $\alpha_{\rm LF}$, satisfying the positivity requirement of section §3.3 in the scalar case, is the largest absolute value of the flux Jacobians in the nodes of an element, which in the system case translates to [1, 53]

$$\alpha_{\rm LF} = \frac{1}{2}\max_{j\in K}(l_j(\|\vec{v}_j^n\| + c_j^n)) \tag{45}$$

with c_j the NLSW celerity (8), and l_j the length of the edge in front of node j. These definitions, combined with equations (27) and (31) give a straightforward two-dimensional generalization of the local Lax-Friedrich's scheme with second order SSP Runge-Kutta time integration, and can be easily shown to preserve the non-negativity of the depth H (see e.g. [49] and [56]). In the scalar case, the scheme verifies the positivity condition (36), and in general yields non-oscillatory solutions.

Unfortunately, the LF scheme is only first order accurate. Indeed, the LF schems does not verify the condition for second order of accuracy recalled in section §2.2. In particular, the relations

$$\beta_i^{\rm LF}\phi^K = \phi_i^{\rm LF} \quad \text{and} \quad \beta_i^{\rm LF}\Phi^K = \Phi_i^{\rm LF}$$

do not define bounded distribution coefficients, and in the system case do not even give enough conditions to determine them, unless some more assumptions are made. The nonlinear Limited Lax Friedrich's (LLF) scheme is obtained as follows (see e.g. [6] for more details)

- Project the LF elemental contributions (43) (or (44) in the corr. step) and the ϕ^K (or Φ^K in the corr. step) onto a basis of the solution space : $\{\ell_m\}_{m=1}^3$. Two possibilities are considered in this paper for ℓ_k (see later) : either the left eigenvectors of the linearized flux Jacobian projected onto the local velocity direction (characteristic projection), or the Euclidean $\mathbb{R}^3$ basis $\{e_m\}_{m=1}^3$, with $e_{mj} = \delta_{mj}$ (limiting equation by equation, no projection). Let

  $$\varphi^{K-m} = \ell_m \cdot \phi^K \quad (\text{or } \varphi^{K-m} = \ell_m \cdot \Phi^K \text{ in the corr. step})$$

  and

  $$\varphi_i^{{\rm LF}-m} = \ell_m \cdot \phi_i^{\rm LF} \quad (\text{or } \varphi_i^{{\rm LF}-m} = \ell_m \cdot \Phi_i^{\rm LF} \text{ in the corr. step})$$

- For each $m \in \{1,2,3\}$, apply a *sign preserving* nonlinear limiter to the otherwise unbounded LF distribution coefficients $\beta_i^{{\rm LF}-m} = \varphi_i^{{\rm LF}-m}/\varphi^{K-m}$. As in [6, 1, 56], the LLF distribution coefficients are computed as

  $$\beta_i^{{\rm LLF}-m} = \frac{\max(0,\, \beta_i^{{\rm LF}-m})}{\sum_{j\in K}\max(0,\, \beta_j^{{\rm LF}-m})} \tag{46}$$

- Redistribute the projected fluctuations as

$$\varphi_i^{\mathrm{LLF}-m} = \beta_i^{\mathrm{LLF}-m}\varphi^{K-m}$$

  Note that the properties of limiter (46) imply that (see e.g. [6, 56] for details)

$$\varphi_i^{\mathrm{LLF}-m} = \beta_i^{\mathrm{LLF}-m}\varphi^{K-m} = \gamma_i\varphi_i^{\mathrm{LF}-m} \quad \text{with} \quad \gamma_i \in [0,\,1] \tag{47}$$

- Project back to physical space

$$\phi_i^{\mathrm{LLF}} = \sum_{m=1}^{3} r_m\beta_i^{\mathrm{LLF}-m}\varphi^{K-m} \quad (\text{or} \;\; \Phi_i^{\mathrm{LLF}} = \sum_{m=1}^{3} r_m\beta_i^{\mathrm{LLF}-m}\varphi^{K-m} \;\; \text{in the corr. step})$$

  with $\{r_m\}_{m=1}^3$ a basis orthonormal to $\{\ell_m\}_{m=1}^3$. Here, the r_m will either be the right eigenvectors of the linearized flux Jacobian projected onto the local velocity direction (characteristic projection), or the Euclidean $\mathbb{R}^3$ basis $\{e_m\}_{m=1}^3$, with $e_{mj} = \delta_{mj}$ (limiting equation by equation, no projection).

The LLF scheme obtained with above procedure is by construction second order accurate, its distribution coefficients being by construction uniformly bounded. Various theoretical results concerning its stability can be found in [6, 1, 56]. Concerning the explicit predictor corrector variant used in this paper, we prove in appendix B the following result.

Proposition 4.7. *Provided that* $\forall\, K \in \Omega_h$ *the Lax-Friedrich's dissipation coefficient verifies*

$$\alpha_{LF} > \max_{x\in K} \|\vec{u}\|_\infty \quad \textit{and} \quad \alpha_{LF} \geq C > 0\,,$$

that the limiting is applied equation by equation, and that it verifies (47) *on the depth equation, for a single* $\gamma_i \in [0,1]$ *in the predictor and corrector steps, then under the time step constraint*

$$\Delta t \leq \min_{i\in\Omega_h} \min\left(\frac{|C_i|}{\sum\limits_{K\in K_i}\alpha_{LF}}, \min_{K\in K_i}\frac{|K|}{3\alpha_{LF}}\right) \tag{48}$$

the explicit LLF scheme preserves the positivity of the depth H*.*

The interest in this proposition is that it provides depth non-negativity preservation conditions very similar to those required for the scheme proposed in [56, 55]. In particular, the time step restriction (48) is roughly a half of the one required for the implicit scheme proposed in the references. Thus, the explicit procedure proposed in this paper represents a definite improvement in terms of efficiency. For more details concerning the construction of nonlinear limited distribution schemes the interested reader is referred to [6, 1, 56] and references therein.

4.4 Filtering and streamline dissipation

While allowing the preservation of depth positivity and a monotone approximation of discontinuous solutions, the LLF scheme suffers from the appearance of weak spurious modes in correspondence of smooth solutions. A thorough analysis of this flaw is made in [1] and is beyond the scopes of this paper. Possible solutions to cure this problem are suggested in [1, 56] for the steady case, and in [56, 8, 53] for the time dependent case. In particular, in [1] it is shown that the spurious modes are related to the ill-posednees of the algebraic equations in smooth regions. The reference also shows

that the discrete equations are always well posed for schemes with a marked upwind character, which is not the case for the LLF scheme. For this reason, the solution suggested in the reference to filter the spurious modes is to add to the scheme a streamline dissipation term of the form [40, 1]

$$\phi_i^{\rm sd} = \delta(u_h)\,{\rm K}_{n_i}\tau\,\phi^K$$

with $\vec{n}_i$ the inward pointing normal to the edge facing node i and scaled by the edge length, with ${\rm K}_{n_i}$ the flux Jacobian projected onto $\vec{n}_i$ (cf. section §2 equations (6) and (7) for the notation), and where the matrix τ is a scaling parameter. Several forms of this parameter are suggested in literature. The interested reader can refer to [40, 56] and references therein for a discussion. In this paper, we have set [1, 56]

$$\tau = \frac{1}{2}|K|\big(\sum_{j\in K}|{\rm K}_{n_j}|\big)^{-1} \tag{49}$$

where the absolute value of the flux Jacobians $|{\rm K}_{n_j}|$ is computed via standard eigen-decomposition. The parameter $\delta(u_h)$ is a scalar smoothness sensor ensuring that the correction is only active in smooth parts of the flow. In particular, $\delta(u_h) < Ch$ across discontinuities, while $\delta \approx 1$ in smooth regions. So the scheme proposed in [1] reads

$$\phi_i = \phi_i^{\rm LLF} + \delta(u_h)\,{\rm K}_{n_i}\tau\,\phi^K$$

Following [53], in this paper we have used the fact that δ is a scalar to define an efficient blending between the linear high order SUPG scheme and the nonlinear high order LLF scheme. The resulting LLFs (Stabilized Limited Lax Friedrich's) distribution reads

$$\phi_i^{\rm LLFs} = (1-\delta(u_h))\phi_i^{\rm LLF} + \delta(u_h)\,{\rm K}_{n_i}\tau\,\phi^K + \frac{\delta(u_h)}{3}\phi^K \tag{50}$$

in the predictor step, and

$$\Phi_i^{\rm LLFs} = (1-\delta(u_h))\Phi_i^{\rm LLF} + \delta(u_h)\,{\rm K}_{n_i}\tau\,\Phi^K + \frac{\delta(u_h)}{3}\phi^K + \delta(u_h)\sum_{j\in K} m_{ij}^{\rm G}\frac{u_j^* - u_j^n}{\Delta t^n} \tag{51}$$

in the corrector step, having denoted by $m_{ij}^{\rm G}$ the standard P^1 Galerkin mass matrix. As remarked in [53], the advantage of (50) and (51) w.r.t. the schemes proposed in [1, 56] is that being both δ and $m_{ij}^{\rm G}$ scalar quantities, at the small additional cost of purely scalar operations a genuinely linear high order scheme is recovered in smooth regions, yielding improved accuracy (see [53] for more).

Concerning the definition of the smoothness sensor $\delta(u_h)$ we have used the one proposed in [56] (see also [1]) :

$$\delta(u_h) = \min\big(1,\ \frac{h_K^2\|E\|_{L^\infty(K)}\|\vec{\nabla}\|_{L^\infty(K)}}{|\varphi_E| + 10^{-12}}\big) \tag{52}$$

where h_K is the local mesh size, E is the NLSW entropy (see e.g. [73, 75, 35, 36], and cf. equation (10) for the notation)

$$E = H\big(\frac{1}{2}gH + gB + {\rm k}\big)$$

while φ_E is an approximation of the entropy residual obtained as

$$\varphi_E = v_K\cdot\phi^K \quad (\text{or } \ \varphi_E = v_K\cdot\Phi^K \ \text{ in the corr. step})$$

with v_K a local averaged value of the symmetrizing variables $\partial E/\partial u$ (cf. section §4.1 and see [34, 73, 75, 35, 36, 56] for details).

4.5 Wet/dry front handling and implementation details

In this last paragraph, we discuss the treatment of the wet/dry fronts, and give some details regarding the implementation of the scheme. As in [56], dry fronts are detected by means of two cut-off constants C_H and $C_{\vec{\mathrm{v}}}$. A node is flagged as dry if $H \leq C_H$. The value of this threshold is set to $C_H = 10^{-12}$. In practice, we have set

$$\phi^K = 0 \quad \text{if } H_j^n \leq C_H \; \forall\, j \in K \quad (\text{and } \Phi^K = 0 \quad \text{if } H_j^n, H_j^* \leq C_H \; \forall\, j \in K \text{ in the corr. step})$$

The second cut-off is instead used to avoid division by zero when computing the local speed $\vec{\mathrm{v}}$. In all computations, we have set $\forall\, i \in \Omega_h$

$$\vec{\mathrm{v}}_i = \begin{cases} \dfrac{\vec{q}_i}{H_i} & \text{if } H_i > C_{\vec{\mathrm{v}}} \\ 0 & \text{otherwise} \end{cases}$$

Furthermore, we have enforced $\vec{q}_i = 0$ if $\vec{\mathrm{v}}_i = 0$. As in [56], the $C_{\vec{\mathrm{v}}}$ cut-off is also used to benefit from the result of proposition 4.7. In particular, following [56], if ϕ_H^K denotes the first component of ϕ^K, and setting $H_{\min} = \min_{j\in K} H_j^n - |\phi_H^K|$, we have set in the computation of the nonlinear LLF distribution coefficients (cf. section §4.3)

$$\ell_m = \begin{cases} \boldsymbol{l}_m & \text{if } H_{\min} > C_{\vec{\mathrm{v}}} \\ e_m & \text{otherwise} \end{cases}, \quad r_m = \begin{cases} \boldsymbol{r}_m & \text{if } H_{\min} > C_{\vec{\mathrm{v}}} \\ e_m & \text{otherwise} \end{cases}$$

with $\boldsymbol{l}_m$ and $\boldsymbol{r}_m$ the m-the left and right eigenvector of the locally linearized NLSW flux Jacobian projected on the local velocity direction. In this way, the limiting is performed equation by equation in elements close to the wet/dry fronts, thus falling in the hypotheses of proposition 4.7. Moreover, to avoid α_{LF} to be zero or too small in these elements, we have set in practice (cf. equation (45))

$$\alpha_{\mathrm{LF}} = \max_{j\in K} l_j \left(\max_{j\in K} (\|\vec{\mathrm{v}}_j\|_{L^\infty} + c_j^n) + \frac{h_K}{L_{\mathrm{ref}}} \right)$$

where the reference length L_{ref} given by

$$L_{\mathrm{ref}} = \max_{i,j\in\Omega_h} \|\vec{x}_i - \vec{x}_j\|$$

As in [56], to take into account the presence of dry fronts the smoothness sensor has been modified as

$$\delta^*(u_h) = \delta(u_h) e^{-\frac{a\, h_K^2}{L_{\mathrm{ref}}^2} \left(\frac{\max_{j\in\Omega_j} H_j^n - C_{\vec{\mathrm{v}}}}{\max(C_H,\, H_{\min} - C_{\vec{\mathrm{v}}})} \right)^2}$$

with $\delta(u_h)$ given by (52). We have experimentally found that the results become insensitive to the choice of a below the value $a = 1/10$, which is the value used in all computations. Concerning the choice of the cut-off $C_{\vec{\mathrm{v}}}$, the interested reader can refer to the numerical tests reported in [56]. Here, following the reference, we have used the mesh dependent value

$$C_{\vec{\mathrm{v}}} = \left(\frac{h}{L_{\mathrm{ref}}} \right)^2$$

Lastly, to preserve the C-property in elements containing dry nodes, we have adopted the bathymetry re-definition suggested in [14], namely

$$B_i = \begin{cases} B(x_i, y_i) & \text{if } H_i > C_H \\ \max\limits_{j\in K,\, H_j > C_H} \eta_j & \text{otherwise} \end{cases}$$

Concerning the quadrature formulas, the elemental fluctuations (23) have been computed using standard Gauss line quadrature to evaluate the contour integrals on triangles boundaries. If not stated otherwise, the standard two points formula has been used (see e.g. [28], chapter 8), which allows to exactly evaluate the H_h^2 term, as required by proposition 4.4. The volume integrals of the friction source term and of the time increment in the residual (28) have been computed by the second order three point formula using the triangles nodes, which is exact for the time increment integrals. Concerning the bathymetry, if not stated otherwise, the integral of $H_h \nabla B_h$ is evaluated exactly for linear H_h and B_h, as required by proposition 4.4. In the super-convergence tests, this integral has been computed as (cf. section §4.1, Lemma 4.1)

$$\int_K H_h \nabla B = |K| \sum_{q=1}^{v_q} \overline{\omega}_q H_h(\vec{x}_q) \nabla B(\vec{x}_q)$$

with ∇B known analytically and with quadrature formulas of different accuracy, taken from [27].

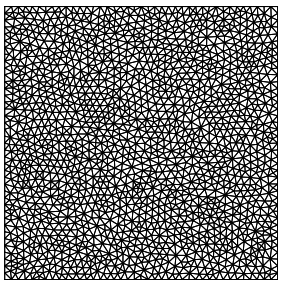

Figure 3: Unstructured grid topology

5 Numerical tests

We discuss in this section the numerical results obtained with the LLFs scheme. Three family of tests are considered : flows on flat bathymetries, C-property tests, wetting/drying tests. The first class of problems will be used to asses the accuracy and shock capturing capabilities of the scheme in absence of bathymetric variations, and to compare computational times with the scheme of [56]. The two different schemes are coded in the same platform, allowing fair comparisons. All the computations have been run on a portable 2.66 Ghz Intel Dual Core PC with 4 GB of RAM memory. In all the computations, the time step has been set to (cf. sections §2 and §4.3)

$$\Delta t = \min_{i \in \Omega_h} \min \left(\frac{|C_i|}{\sum\limits_{K \in K_i} (\alpha_{\rm LF} + \max\limits_{j \in K} g c_{\rm f}(u_j^n))}, \min_{K \in K_i} \frac{|K|}{3\alpha_{\rm LF} + \max\limits_{j \in K} g c_{\rm f}(u_j^n)} \right)$$

for the LLFs proposed here, while for the scheme of [56] we have used the maximum time step allowed for depth non-negativity :

$$\Delta t = 2 \min_{i \in \Omega_h} \min_{K \in K_i} \frac{|K|}{3\alpha_{\rm LF}}$$

5.1 Flows on flat bathymetry

5.1.1 Vortex transport, accuracy and efficiency

We consider the traveling vortex problem proposed in [56] to test the accuracy of the scheme. The exact solution consists of the advection along the x-direction of a vortex described by an analytical perturbation of H and $\vec{\mathrm{v}}$ about a constant state $H = 10\,[m]$ and $\vec{\mathrm{v}} = (6,\, 0)$ (see [56] for details). The spatial domain is the square $[0,\, 1]^2$, with periodic boundary conditions in the x direction. Numerical solutions are computed at time $T = 1/6$, corresponding to the moment in which the vortex has crossed the whole domain and gotten back in its initial position, due to the periodic boundary conditions. The computations have been performed on 4 unstructured grids with the topology shown on figure 3. The coarsest mesh has size $h \approx 1/56$. The other 3 meshes have been generated independently, halving the mesh size at each step.

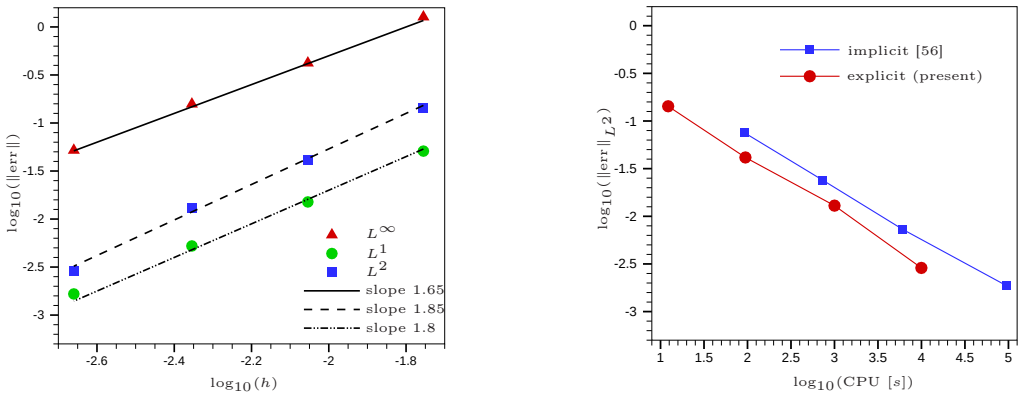

Figure 4: Vortex trasport. Grid convergence for the explicit scheme (left), and error-CPU time comparison between explicit and implicit scheme [56]

We present the results on figure 4. The left picture, in particular, shows the grid convergence history of the error, confirming the theoretical second order of accuracy. The right picture, instead, shows the evolution of the L^2 norm of the error w.r.t CPU time, measured in seconds. The plots compares the results of the explicit LLFs scheme proposed here, with those of the implicit scheme of [56]. The plot shows that on a given mesh, the scheme of the reference provides a lower error, however, the computational times required are roughly 6 or 7 times larger than those of the explicit scheme proposed here. In particular, for a given error level, the explicit scheme we propose is roughly 4 times faster than the reference.

5.1.2 Asymmetric break of a dam

This test, taken from [67, 54], consists of the asymmetric break of dam separating two basins with water depths of 5 and 10 meters. The dam is contained in the computational domain $[0,\, 200]^2$, and the breaking is initially placed at $x = 95\ [m]$. Reflective boundary conditions are used on all boundaries. A sketch of the geometry and a close up view of the mesh are reported on figure 5. The mesh size is $h \approx 2[m]$, the mesh contains 19274 triangles and 9899 nodes. We refer to [67, 54] for more details on the test set up. Computations have been run up to time $T = 7.2\ [s]$ with the explicit LLFs scheme proposed here and with the scheme of [56]. Results are summarized on figures 6 and 7.

Figure 5: Asymmetric dam break. Left: computational domain. Right: mesh close up ($h \approx 2$)

In particular, figure 6 shows 3D visualizations of the free surface level computed with the explicit LLFs scheme proposed here, and the one obtained with the implicit scheme of [56]. The scheme of [56] provides slightly sharper shocks and stronger rarefactions around the corners, as shown by presence of more pronounced kinks in the depth contours in the region of the trough forming in the emptying basin from the interaction of the two corner rarefactions. Similar observation can be made by looking at the depth and Froude number profiles on figure 7. The plots compare the data along the line $y = 132[m]$, which is roughly the position of the center of the depth trough due to the interaction of the corner rarefactions (cf. left picture on figure 5). We se again that the implicit scheme provides slightly sharper shocks, while the effect of the stronger corner rarefactions are particularly visible in the deeper trough in depth and higher peak in Froude number at $x \approx 55[m]$. The differences between the two solutions are however not striking. On the other hand, the computational times required to obtain the solutions ore of 53.3 $[s]$ for the explicit scheme proposed here, and of 331 $[s]$ for the scheme of [56], which is more than 6 times larger. This shows again the improvement brought by the scheme proposed here.

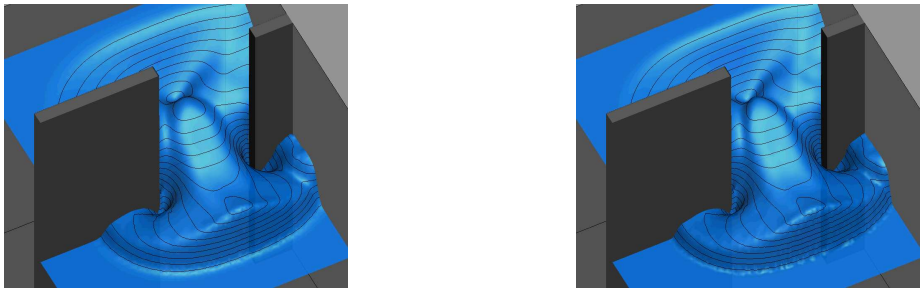

Figure 6: Asymmetric dam break: water height at time $t = 7.2$. Left: explicit scheme. Right: implicit scheme of [56]

5.2 C-property tests

5.2.1 Lake at rest solution

We start by considering the lake at rest solution. In particular we consider 2 benchmarks allowing to verify numerically proposition 4.4. On the spatial domain $[0, 2] \times [0, 1]$, let the bathymetry be defined as :

$$b(x, y) = b_0 e^{\psi(x,y)}$$

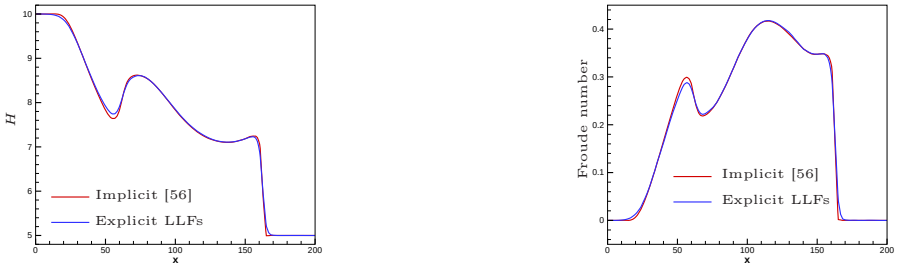

Figure 7: Asymmetric dam break: water height (left) and Froude number (right) at time $t = 7.2$. Data extracted along the line $y = 160$

In particular, we consider two cases. The first definition is obtained with

$$b_0 = 0.8 \quad \text{and} \quad \psi = -5(x-0.9)^2 - 50(y-0.5)^2$$

This definition is used in a large number of references to verify the C-property (see e.g. [77, 67, 42] and references therein). We also consider the following non-smooth case, proposed in [54] :

$$b_0 = 0.6 \quad \text{and} \quad \psi = \begin{cases} \sqrt{(x-0.9)^2 + (y-0.5)^2} & \text{if } \vec{x} \in [0.9,\, 1.1] \times [0.3,\, 0.7] \\ -5(x-0.9)^2 - 50(y-0.5)^2 & \text{otherwise} \end{cases}$$

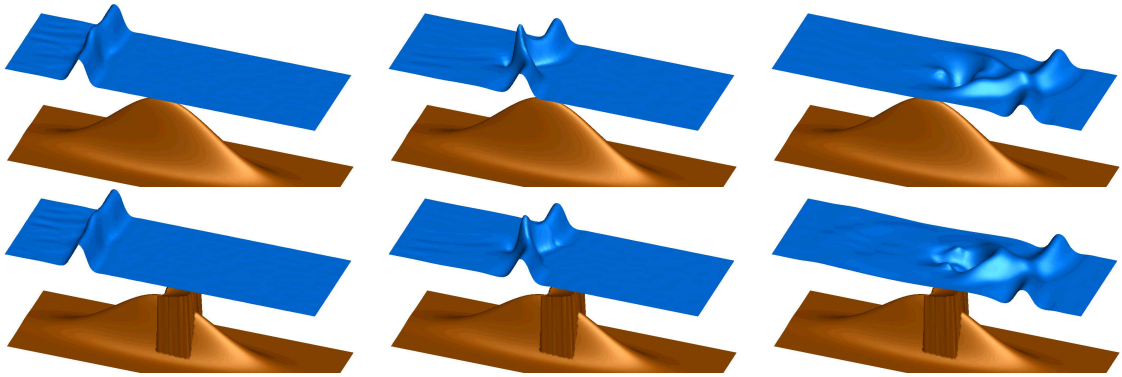

Figure 8: Small perturbation of lake at rest: 3d view of total water height at times $t = 0.12$ (left), $t = 0.24$ (middle), and $t = 0.48$ (right). Explicit LLFs scheme with smooth (top row) and non-smooth (bottom row) bathymetry

For both definitions, we have run the explicit LLFs scheme with the initial lake at rest solution $(\eta,\, q) = (1,\, 0)\ \forall\, \vec{x} \in \Omega$. As foreseen by proposition 4.4 the results are constant up to machine accuracy. To visualize this fact, we consider an perturbation of the lake at rest state given by $\vec{q} = 0$, and

$$\eta_0(x, y) = \begin{cases} 1.01 & \text{if } x \in [0.05,\, 0.15] \\ 1 & \text{otherwise} \end{cases}$$

With this initial condition we have run the LLFs scheme on a mesh with typical size $h \approx 1/00$, containing 20037 nodes and 39472 triangles. The results obtained on the smooth and non-smooth bathymetry are visualized in terms of 3d view of the free surface η (and bathymetry B) on figure 8, of 1d line plots of the data extracted along the line $y = 0.5$ (both η and bathymetry) on figure

9, and of contours of the free surface η on figure 10. In all pictures, the bathymetry is rescaled to allow properly visualizing the free surface.

The results show the perfect preservation of the initial lake at rest state away from the perturbation. The features captured by the scheme proposed here match quite well those of other results presented in published literature (see e.g. [77, 67, 42, 54, 56] and references therein), confirming both the well balanced character and the accuracy of the scheme proposed.

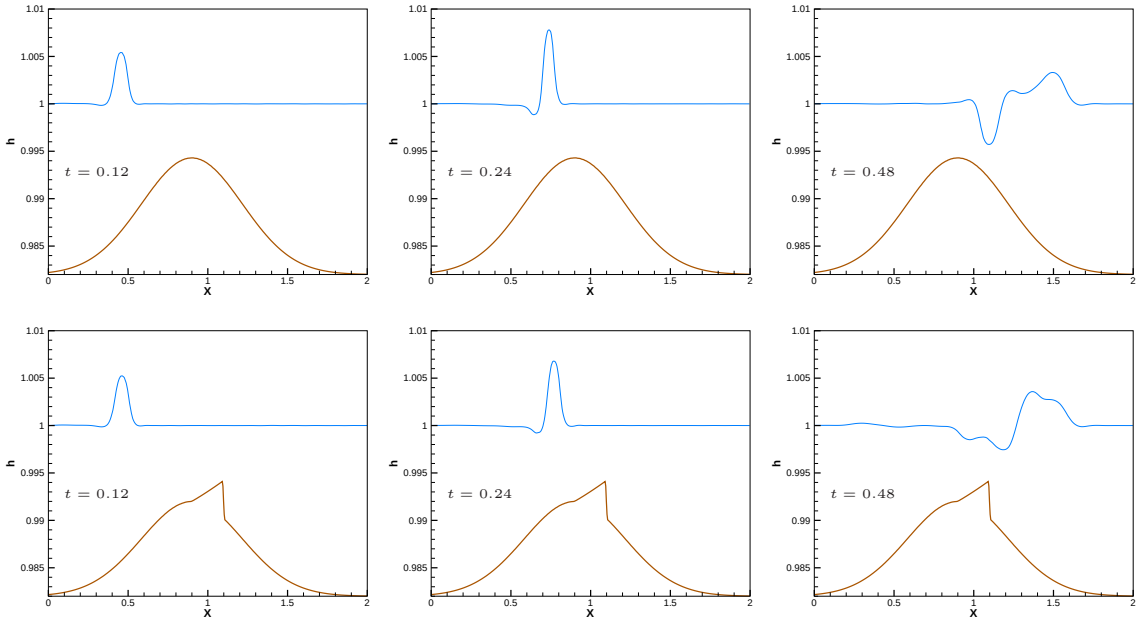

Figure 9: Small perturbation of lake at rest: line plot of total water height at times $t = 0.12$ (left), $t = 0.24$ (middle), and $t = 0.48$ (right). Explicit LLFs scheme with smooth (top row) and non-smooth (bottom row) bathymetry. Data extracted along the $y = 0.5$ line

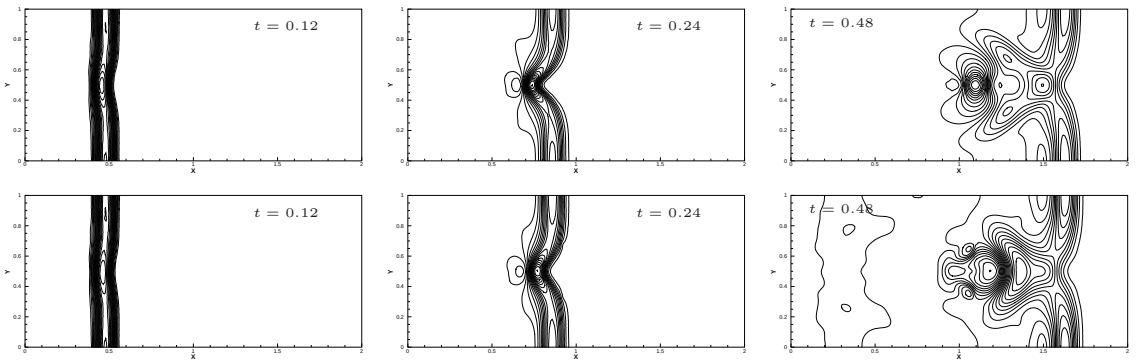

Figure 10: Small perturbation of lake at rest: contour plot of total water height at times $t = 0.12$ (left), $t = 0.24$ (middle), and $t = 0.48$ (right). Explicit LLFs scheme with smooth (top row) and non-smooth (bottom row) bathymetry.

5.2.2 Constant energy flows

In this section we check numerically the super-consistency property of propositions 4.2 and 4.5. Following [52], we consider, on the square $[0, 25]^2$, the pseudo one-dimensional bathymetry

$$b(x, y) = \begin{cases} f(x) & \text{if } x \in [8,\, 12] \\ 0 & \text{otherwise} \end{cases}$$

The function $f(x)$ is chosen with increasing regularity. We start with the C^0 definition

$$f(x) = 0.2 - (x - 10)^2/20 \tag{53}$$

giving a H^1 bathymetry, and then consider

$$f(x) = 0.2 \, \sin^{2l}(\pi(x - 8)/4)\,, \quad l \in \{1,\, 2,\, 4\} \tag{54}$$

yielding H^{2l} bathymetries with C^{2l-1} continuity. We compute initial nodal values from (15), with $\mathcal{E}_0 = 22.06605$ and $\vec{q}_0 = (4.42, 0)$, and run unsteady computations until time $T = 0.1\,[s]$ on four nested unstructured grids with the topology shown on figure 3. To fit into the hypotheses of propositions 4.2 and 4.5, in all computations we use the spatial approximation $\boldsymbol{\mathcal{F}}_h = \boldsymbol{\mathcal{F}}(u(v_h, b))$ and $\boldsymbol{\mathcal{S}}_h = \boldsymbol{\mathcal{S}}(u(v_h, b), \nabla b)$, with b the analytical bathymetry, and $v_h = (\mathcal{E}_h,\, \vec{q}_h)$ linear. The runs are repeated with different quadrature strategies. Edge integrals are computed with formulas exact for polynomial degrees $f = 1$, 3, and 11. Two-dimensional integration formulas on triangles exact for polynomial degrees $v = 1$, 4, and 6 are taken from [27]. We discuss the results obtained with the four strategies :

$$\mathrm{Q}_1 :\ f = 1,\, v = 1; \quad \mathrm{Q}_2 :\ f = 3,\, v = 4; \quad \mathrm{Q}_3 :\ f = 11,\, v = 4; \quad \mathrm{Q}_4 :\ f = 11,\, v = 6$$

Recall that for a H^{p+1} bathymetry, with sufficiently large p, the accuracy measured for a finite time computation should be, according to propositions 4.2 and 4.5,

$$\epsilon = \mathcal{O}(h^l) \ \text{ with } \ l = \min(f + 1\, v + 2) \tag{55}$$

which gives for the four quadrature strategies considered the theoretical slopes

$$l_1 = 2, \ \ l_2 = 4, \ \ l_3 = 6, \ \ l_4 = 8$$

The numerical results are shown on figure 11. In the figure, the first four pictures on the first and second column represent the grid convergence of the depth at $t = 0.1\,[s]$. The last two pictures show the error convergence on a fixed grid (the coarsest on top, the finest on the bottom) when increasing the accuracy of the quadrature. Below each picture, we have reported the quadrature strategy used, and the expected theoretical slope. We recall that the explicit LLFs scheme used is formally second order accurate.

We can see that the discrete solution at time $T = 0.1\,[s]$ super converges if the bathymetry is regular enough. The theoretical slopes of the propositions are recovered for the smoothest bathymetry. As anticipated at the end of section §4.1, when the regularity of $b(x, y)$ gets lower the accuracy saturates at an order l given by (42). In particular, only first order of accuracy is observed if $b \in H^1$. The degree of super convergence depends also on the quadrature formula. In particular the rightmost column on figure 11 shows the error reduction for the different quadrature formulas on the coarsest and finest meshes used in the grid convergence study. Not that the x-axis in these pictures has no quantitative meaning, except that the accuracy of the edge, and/or volume quadrature increases from left to right. These plots confirm that the error indeed converges to zero (towards exact preservation) if the quadrature accuracy is increased. The smoother the bathymetry,

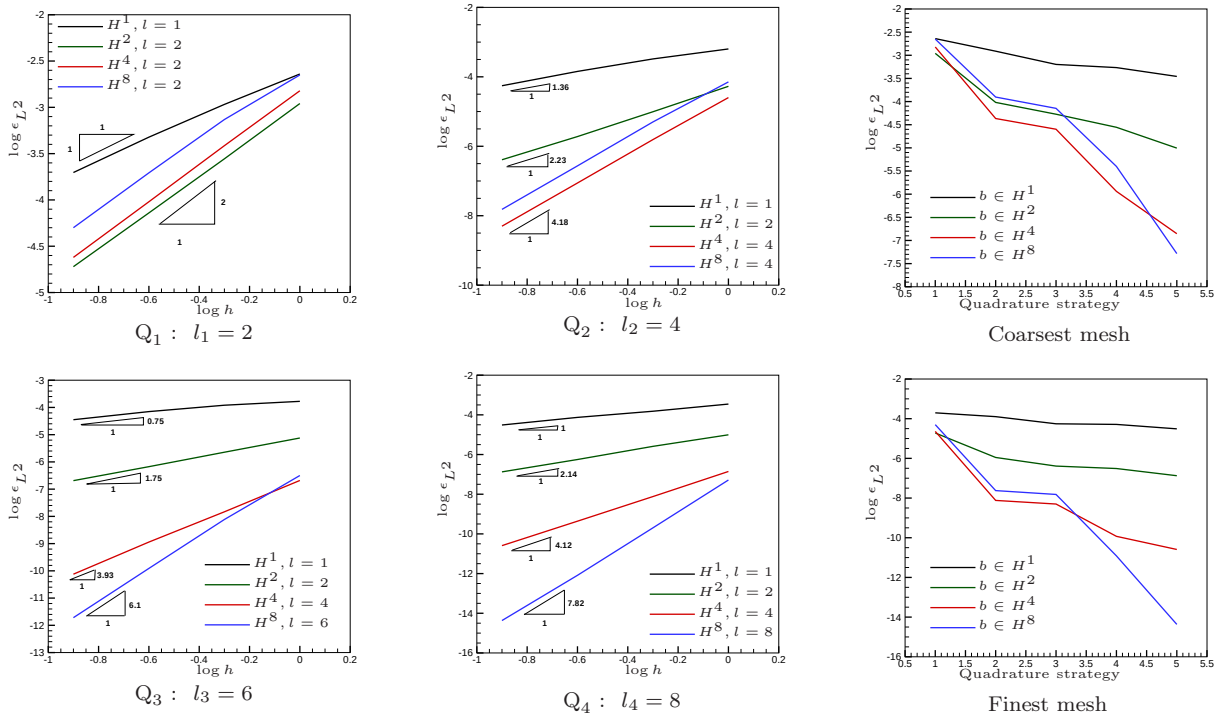

Figure 11: Super consistency for constant energy flows : grid convergence (left and middle columns) and quadrature convergence (rightmost column) of the depth error.

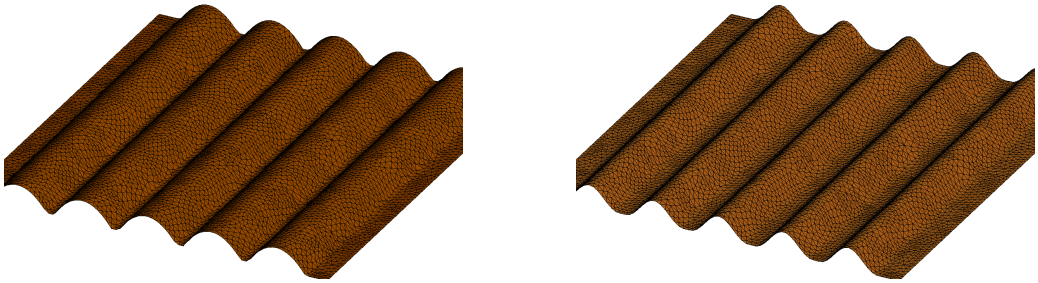

Figure 12: Ribbed channel bathymetries. Left : C^0 piecewise parabolic. Right : C^1 piecewise $\sin^2$

the faster the convergence. The interested reader can refer to [52] for similar results obtained with the scheme of [56], and also for the lake at rest case.

To show *visually* the benefits of using our residual approach in conjunction with the approximation in total energy variables, we consider the perturbation of a pseudo one dimensional flow on a bathymetry representative of a ribbed channel. In particular, we consider on the square $[0, 25]^2$ a series of 5 ribs starting at $x = 1.5$, 6, 10.5, 15, and 19.5 $[m]$. Two rib shapes are considered : a C^0 picewise parabolic definition obtained by shifting (53), and a C^1 definition obtained shifting (54) with $l = 1$ ($\sin^2$ ribs). The bathymetries obtained are visualized on figure 12. In the pictures we also show the mesh used in the computations, containing 6553 nodes and 12784 elements ($h \approx 25/80$). We then consider a supercritical solution obtained from (15) setting the value of the

gravity acceleration to $g = 1\,[m/s^2]$, and with $\mathcal{E}_0 = 6$, and $\vec{q}_0 = (5.65685, 0)$. Let η_{steady} be the free surface level associated to this initial solution. Next, following [47], we perturb the total energy $\mathcal{E}$ in the box $[6.5, 7.5] \times [12, 13]$, adding the perturbation $\delta\mathcal{E} = 0.1$. We then compute the evolution of the perturbation until time $t = 2\,[s]$ (recall that the we have set $g = 1\,[m/s^2]$) with the explicit LLFs scheme proposed here, using either the standard approximation in $[H_h, \vec{q}_h]$ variables with a piecewise linear approximation of the bathymetry b_h, or using the approximation of propositions 4.2 and 4.5 : $\boldsymbol{\mathcal{F}}_h = \boldsymbol{\mathcal{F}}(u(v_h, b))$ and $\boldsymbol{\mathcal{S}}_h = \boldsymbol{\mathcal{S}}(u(v_h, b), \nabla b)$, with b the analytical bathymetry, and $v_h = (\mathcal{E}_h, \vec{q}_h)$ linear.

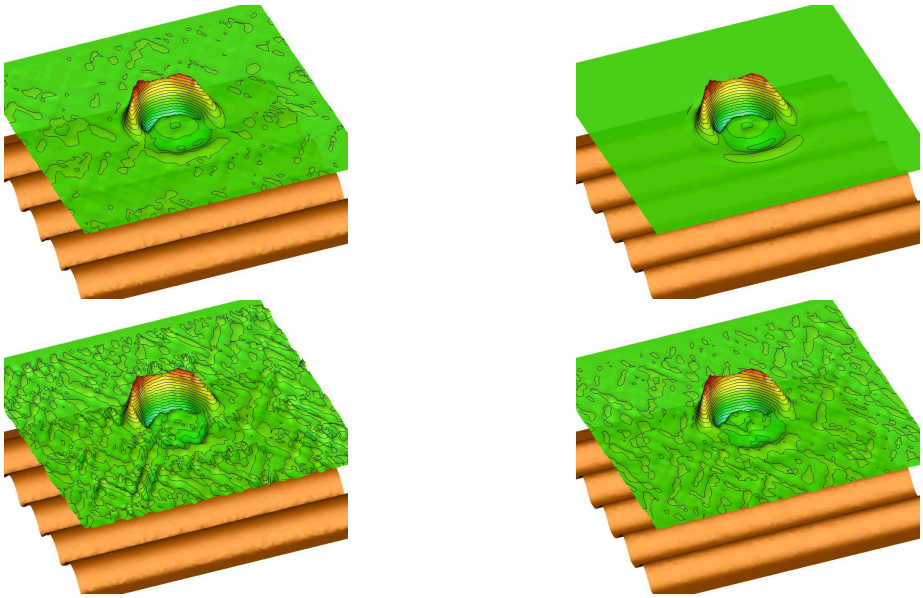

Figure 13: Perturbation of constant energy state states. Free-surface perturbation $\eta - \eta_{\text{steady}}$ at time $t = 0.4s$. Left pictures : C^0 bathymetry (discontinuous derivative). Right pictures : C^1 bathymetry. Top : approximation in $[\mathcal{E}, \vec{q}]$ with analytical b. Bottom : approximation in $[H, \vec{q}]$ with linear b_h

The results obtained are reported on figures 13 and 14. In particular, on figure 13 we report an exaggerated 3d view of the free surface level perturbation $\eta - \eta_{\text{steady}}$ for the C^0 bathymetry (left column) and for the C^1 case (right column). The top results are obtained with the approximation in total energy variables, verifying the hypotheses of propositions 4.2 and 4.5, while the results on the bottom row are obtained with a standard approximation in $[H_h, \vec{q}_h]$ variables. The figures clearly show that even if formally only first order accurate, even for a C^0 bathymetry, the approximation in total energy variables provide a much better preservation of the undisturbed steady state. The results obtained for the C^1 bathymetry show that the preservation of the steady solution is practically perfect when using total energy variables, the deviation being of the order of 10^-8. To confirm these observations, on figure 14 we report in the top row the one-dimensional distribution of the free surface perturbation $\eta - \eta_{\text{steady}}$ along the line $y = 12.5$, and in the bottom row the 1d plot of $\eta - \eta_{\text{steady}}$ in *all the mesh points in the box* $[0, 6] \times [0, 25]$. The left column shows the results obtained on the C^0 bathymetry, while the results of the C^1 case are reported on the right column. The top pictures show that the result obtained using total energy variables (red curves) is smoother in both cases, with much smaller deviation from zero in the undisturbed region (left most and rightmost ends of the domain) in the C^0 case, and clearly no visible deviation from the steady state in the C^1 case. The data reported in the pictures on the bottom confirm this last

observation : in the C^0 case (left picture) the results in total energy variables (red curve) are much more clustered around zero, the largest peaks being of the order of one third of those of the standard approximation. On the other hand, the right picture confirms that in the C^1 case the preservation of the steady state is practically perfect.

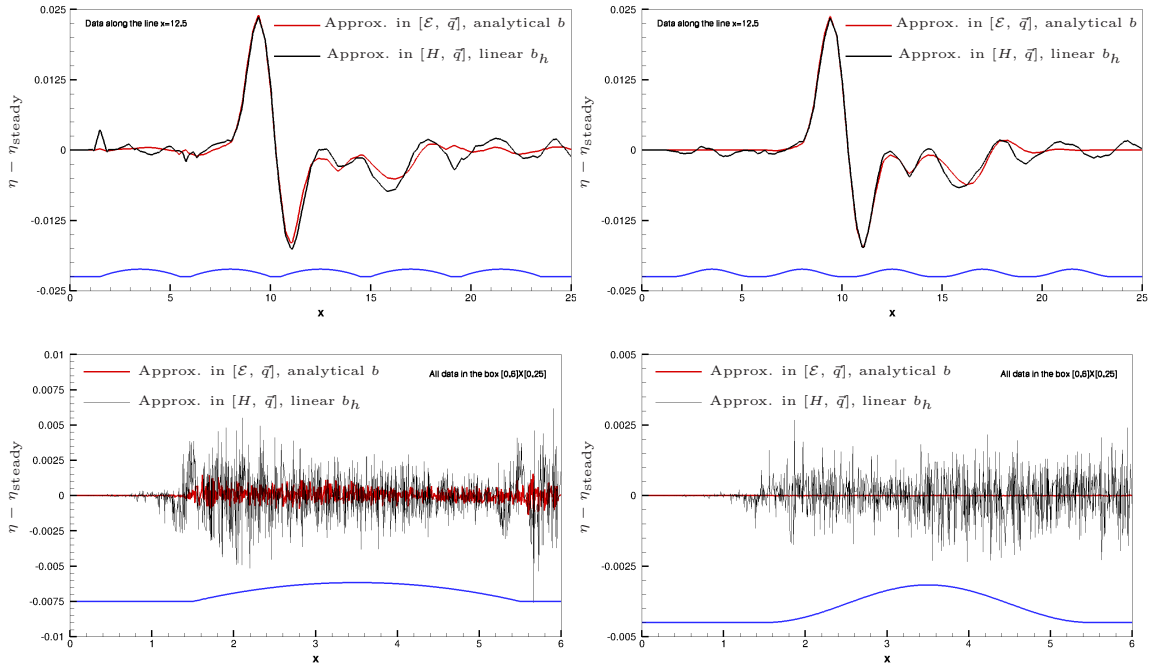

Figure 14: Perturbation of constant energy state states. Free-surface perturbation $\eta - \eta_{\text{steady}}$ at time $t = 0.4s$. Left : C^0 bathymetry (discontinuous derivative). Right : C^1 bathymetry. Top : data extracted along the line $y = 12.5$. Bottom : all data in the "unperturbed" box $[0, 6] \times [0, 25]$.

Remark 5.1 (Bathymetry representation)**.** *The results shown, as well as the theoretical developments, are based on the assumption that an analytical bathymetry is available, and that its exact form is used in the discretization. The availability of such a bathymetry is of course questionable. However, given the uncertainties in the experimental data providing such quantity, it seems reasonable to think of a pre-processing step building a C^1 continuous spline (or some other smooth polynomial) representation of the data, thus giving some space for application of the method where this type of flow is relevant.*

Concerning bathymetries with less regularity, an inspection of equations (14) *suggests that the real information needed to correctly reproduce these solutions is $\vec{v}^{\perp} \cdot \nabla b = 0$. This type of condition is very easily reproduced on structured meshes, as shows by the analysis made in [54]. On unstructured grids, the use of total energy variables interpolation leads to first order of convergence, however, the results shown here demonstrate that the magnitude of the error is still smaller that that obtained in standard variables, which however allows to recover second order rates [56, 55].*

5.2.3 Flows in sloping channels with friction

We present a verification of proposition 4.6. On the square $[0, 1]^2$, we consider a rotated solution of the type (19), with a bathymetry obtained as $b = b_0 - \xi x^*$, with $x^* = (2x+y)/\sqrt{5}$. We then compute

two solutions from (19) corresponding to a sub-critical (Fr ≈ 0.638) and super-critical (Fr ≈ 2.536) flow. We then perturb the free surface level by $\delta\eta = 0.01$ within the circle centered in (0.5, 0.5) and of radius $r = 0.1$. We compute the evolution of the perturbation with the explicit LLFs proposed here, using a standard approximation in $[H_h, \vec{q}_h]$ variables, on an unstructured triangulation similar to that shown on figure 3, and containing 6553 nodes and 12784 elements ($h \approx 1/80$).

A three-dimensional visualization of the evolution of the perturbation $\eta - \eta_{\text{steady}}$ is reported on figure 15. The results clearly show the perfect preservation of the underlying steady state.

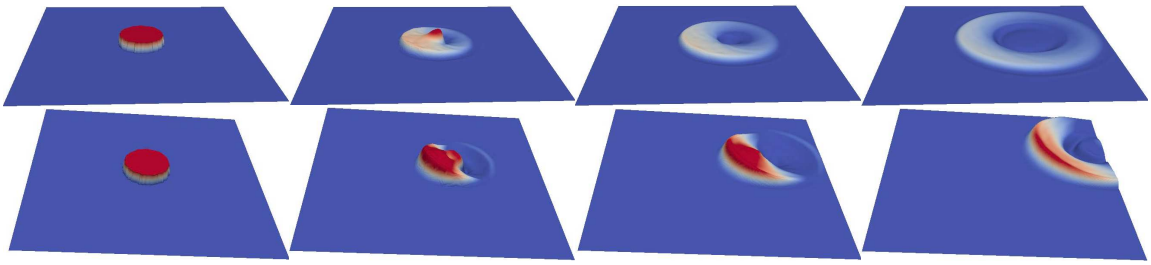

Figure 15: Flows in sloping channels with friction. Evolution of a free surface perturbation in the sub-critical (top row) and super-critical (bottom row) cases.

5.3 Wetting/drying tests

5.3.1 Thacker's oscillations in a parabolic bowl

We consider first a simple test to verify the capability of the scheme to provide an accurate and stable approximation of moving shorelines. The test is one of the two analytical solutions to the frictionless NLSW equations given in [76], and consists of periodic oscillations of the free surface in a paraboloidal bowl. Details concerning the definition of the bathymetry and the exact analytical solutions can be found in the reference. We consider here two tests. In the first, we set the free surface to the analytical solution at time $t = 0$ and let it oscillate for three full periods. We then look at the solution at times $3T + \delta t$ for $\delta t \in \{T/6, T/3, T/2, 2T/3, 5T/6, T\}$. The spatial domain $[-1.2, 1.2]^2$ is discretized with un unstructured triangulation with the topology shown on figure 3 containing 10113 points and 19824 elements, and with size $h \approx 1/40$, which gives roughly 50 cells along the diameter of the oscillating region.

The data along the line $y = 0$ computed by the LLFs scheme proposed here is compared to the exact solution on figure 16. The computed solutions are nicely close to the analytical ones, even on this relatively coarse mesh. The close ups of the wetting/drying region reported on the left column also show a clean and oscillation free capturing of the moving shoreline.

Next we have compared the results obtained with the explicit LLFs scheme proposed here with those obtained with the scheme of [56]. The accuracy of the two schemes is compared in terms of L^1 norm of the error on the free surface after one period in figure 17. We can see that, while the slope obtained with the scheme of [56] is closer to 2, the absolute value of the error of the scheme proposed here is significantly lower. Moreover, the CPU time required for one period on the $h = 1/40$ mesh, containing 10113 points and 19824 elements, is of 103.470 $[s]$ for the explicit LLFs proposed here, and of 13 minutes and 33.110 $[s]$ for the implicit scheme of [56]. This further confirms the significant improvement brought by the present work.

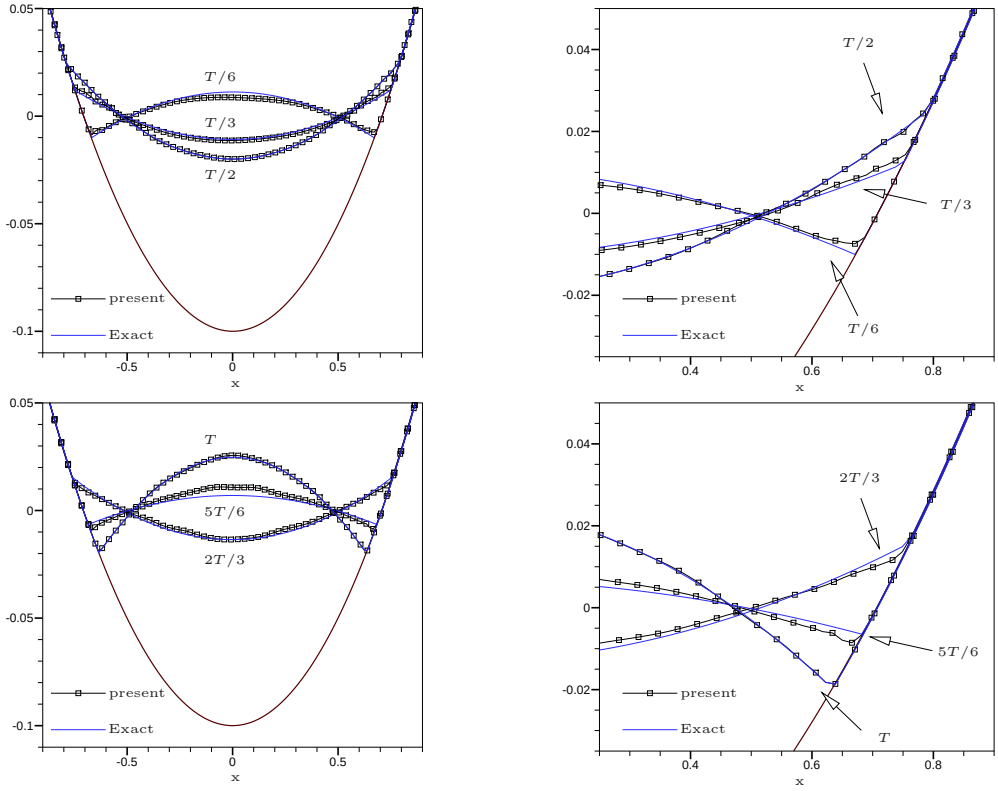

Figure 16: Periodic oscillations in a parabolic bowl [76]. Free surface level at times $3T + \delta t$ for $\delta t \in \{T/6, T/3, T/2, 2T/3, 5T/6, T\}$. Data along the line $y = 0$ compared with exact solution [76]

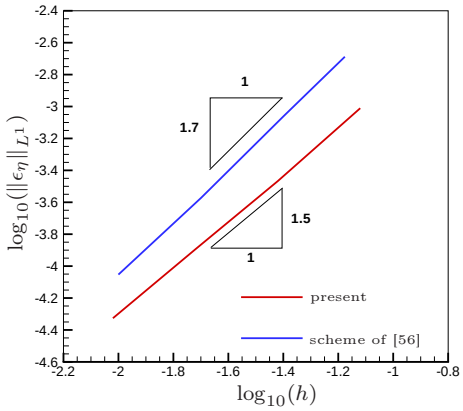

Figure 17: Periodic oscillations in a parabolic bowl [76]. Grid convergence and comparison with the scheme of [56]

5.3.2 Runup on a conical island

This is a standard test to validate the ability of a scheme to correctly predict long wave run up. The test aims at reproducing the experiments performed in [13]. A sketch of the test is depicted on the left figure 18 : a solitary wave travels over a island of conical shape. The experiments of [13] have provided both point wise time series of the water level in the gauge points indicated in figure 18, and the maximum run up heights over the island. For more details the interested reader is referred to [13].

The computational domain used to reproduce the test is the rectangle of $[-12.96, 12.4] \times [-13.8, 16.2]$ with the center of the island placed in the origin of the axes. The islands lower radius is $3.6\,[m]$, the upper one is $1.1\,[m]$ and the slope $1/4$ with a peak height of $0.625\,[m]$. We have considered the case in which the water depth far from the island is $h_0 = 0.32\,[m]$. The solitary wave shape imposed at the left hand of the domain is defined by the free surface perturbation

$$d\eta = A\,\mathrm{sech}^2(\sqrt{3A/(4h_0^3)}x)$$

with a corresponding velocity perturbation obtained from the linearized Shallow Water equations : $\vec{\mathrm{v}} = (\sqrt{g/h_0},\, 0)d\eta$. We consider here the case of a soliton of amplitude $A = 0.2$. The spatial domain is discretized with an unstructured triangulation. On the right on figure 18 we report a view of the mesh which is refined around the island. The largest mesh size is of 50 [cm], while the finest is of 7.5 [cm]. For better understanding, the picture also shows the lower and upper circles of the island, and the positions of the four gauges which will be used for validation :

$$g6 = (-3.6, 0)\,, \quad g9 = (-2.6, 0)\,, \quad g16 = (0, -2.58)\,, \quad g22 = (2.6, 0)$$

The mesh dependent cut-off coefficients needed for the wet-dry treatment (cf. section §4.5) are computed using a local mesh size.

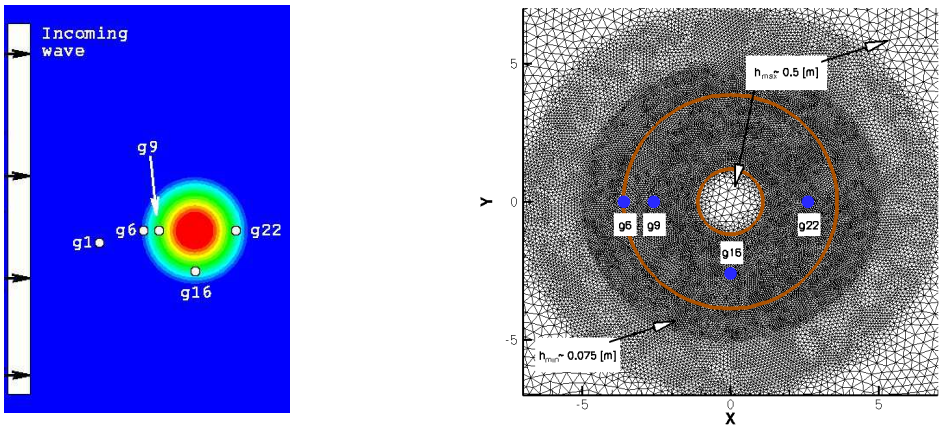

Figure 18: Run up on a conical island [13] : problem sketch (left) and computational grid (right)

An exaggerated three-dimensional visualization of the run up process is presented in figure 19. The pictures show the soliton run up first on the front side of the island, then the secondary waves running around the island and meeting behind it giving the rear side run up visible in the leftmost picture on the bottom row. The rear wave then splits again into two smaller waves running back around the island.

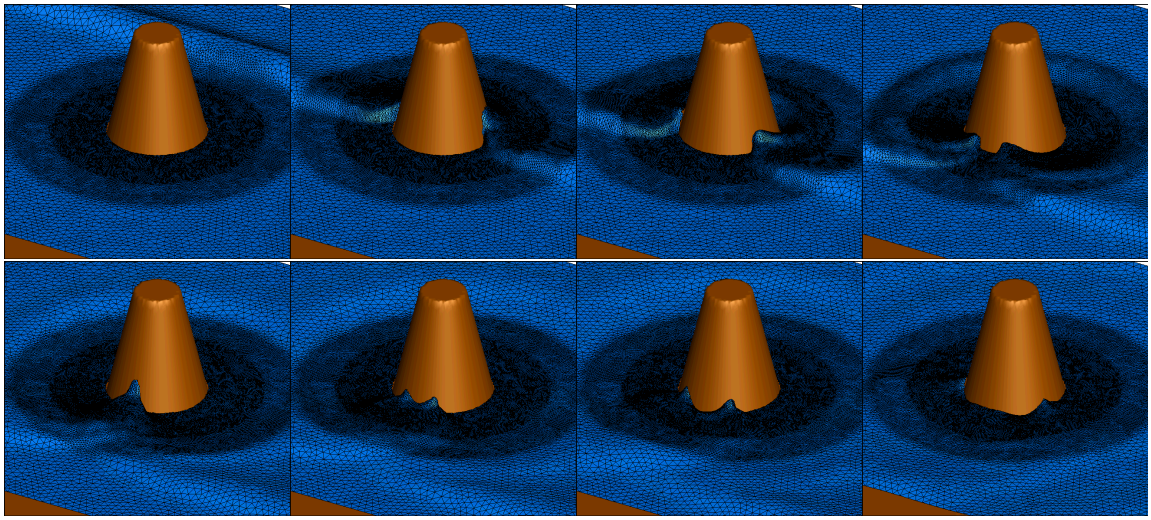

Figure 19: Run up on a conical island [13] : three-dimensional visualizations of free surface evolution (from left to right and from top to bottom).

On figure 20 we report the comparison with the experimental data [13] of the computed time history of the water height deviation $\eta - \eta_0$, η_0 being the free surface level at still water. The results of the explicit LLFs scheme proposed match quite well the experimental data, within at least the limits of the capabilities of the NLSW model. Non-hydrostatic terms are needed to better match the oscillations seen e.g. in gauge g9 after the backwash phase (around time $t = 10\,[s]$). To further confirm the soundness of the wetting/drying procedure, on figure 21 we compare the maximum run up with the data of [13]. To obtain the figure we have superposed the solutions at all times and then blanked the cells in which the minimum depth is below $10^{-5}\,[m]$. This value has been set by trial and error. Using smaller values, results in the random appearance of "wet" cells not connected to the rest of the domain, as already visible un the top part of the figure. The boundary of the wet region computed by our scheme is in excellent agreement with the experiments.

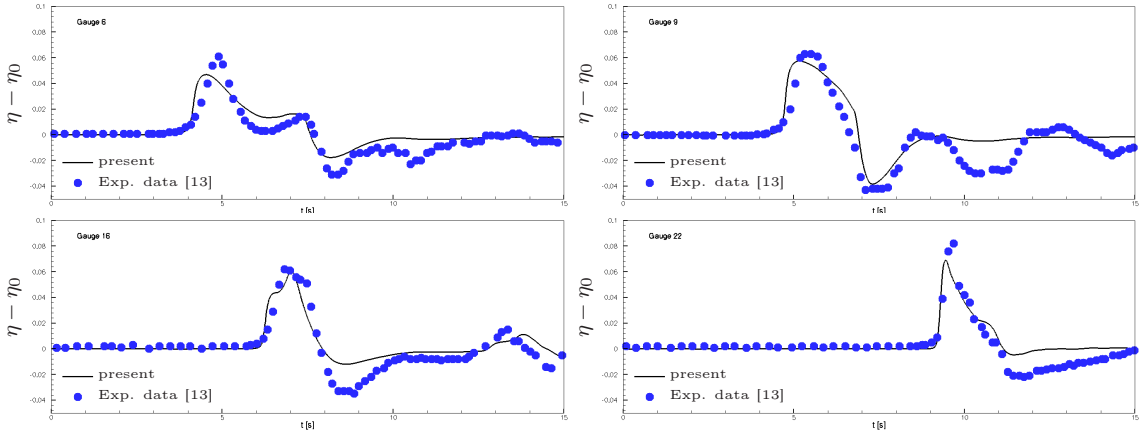

Figure 20: Run up on a conical island [13] : gauge data (left)

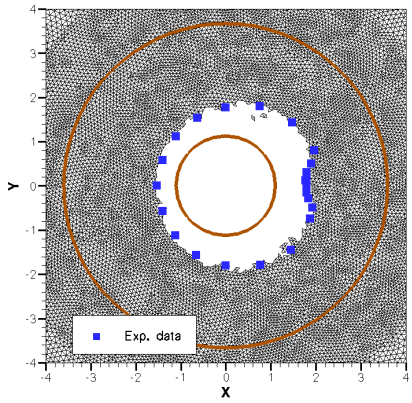

Figure 21: Run up on a conical island [13] : maximum run up plot

5.3.3 Okushiri tsunami experiment

As a final application we consider the second benchmark of the third international workshop on long wave runup models : Tsunami runup onto a complex three-dimensional beach. The test is thoroughly described on the web page `http://isec.nacse.org/workshop/2004_cornell/index.html` to which we refer for details. The interested reader can also consult the volume [43]. The test is a scaled down laboratory reproduction of the tsunami wave that hit the Okushiri island in Japan in 1993. The web page provides data files for the bathymetry of the coast of the island in the region of the Monai village, which is the one where the most damage has been observed. A three-dimensional view of the bathymetry is reported on the left picture on figure 22. On the figure, the highest point (about $50\,[m]$ in real life) is the Monai village region while the small island in front of the coast is the Muen island reaching $10\,[m]$ height in real life. The web site gives a 400 times scaled down geometry together with the shape of the wave used in the experiment, which is reported on the right on figure 22.

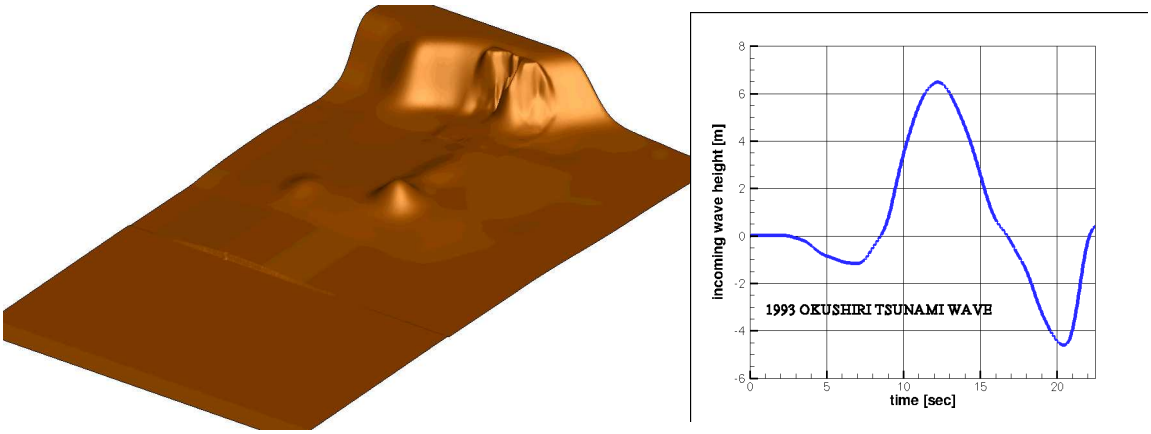

Figure 22: The Okushiri Tsunami experiment. Left : bathymetry. Right : inlet wave

The spatial domain has been discretized with two meshes, both adapted to the bathymetric variations. A close up view of the meshes is reported on figure 23. The coarse mesh (left picture) contains 7000 nodes and 13720 triangles, with maximum and minimum mesh sizes given roughly by $0.1\,[m]$ and $0.025\,[m]$. The fine mesh (right picture) contains 18711 nodes and 36911 triangles, with

maximum and minimum mesh sizes given roughly by $0.05\,[m]$ and $0.01\,[m]$. Simulations have been run with the LLFs scheme for $25\,[s]$, using local mesh sizes to compute the cut-off thresh-holds for the wetting/drying treatment (cf. section §4.5). Three-dimensional visualizations of the computed flow are reported on figure 24.

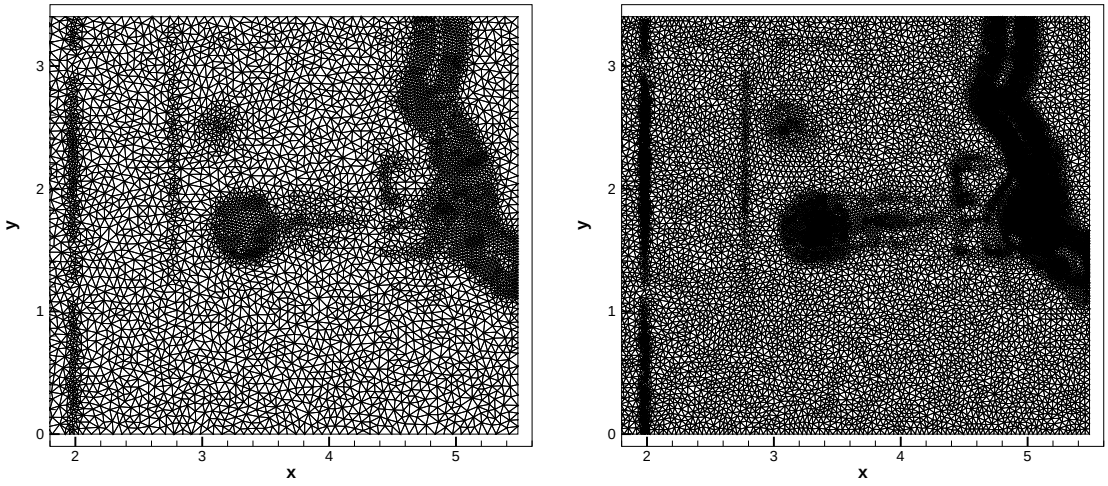

Figure 23: The Okushiri Tsunami experiment. Left : coarse adaptive mesh ($h_{\min} \approx 0.025$ and $h_{\max} \approx 0.1$) bathymetry. Right : fine adaptive mesh ($h_{\min} \approx 0.01$ and $h_{\max} \approx 0.05$)

The pictures (from left to right and from top to bottom) show the initial withdrawing of the water followed by the arrival of the main wave (top row). After hitting the beach, the wave reflects, and a large wave travels toward the right to hit the steepest slopes in the region of the Monai village (bottom row, third picture from the left). The reflected wave eventually reaches and inundates the Muen island (bottom row last picture from the left). The highest height reached by the water in the experiment is about $32\,[m]$ in real life (corresponding to $32/400\,[m]$ in the scaled model).

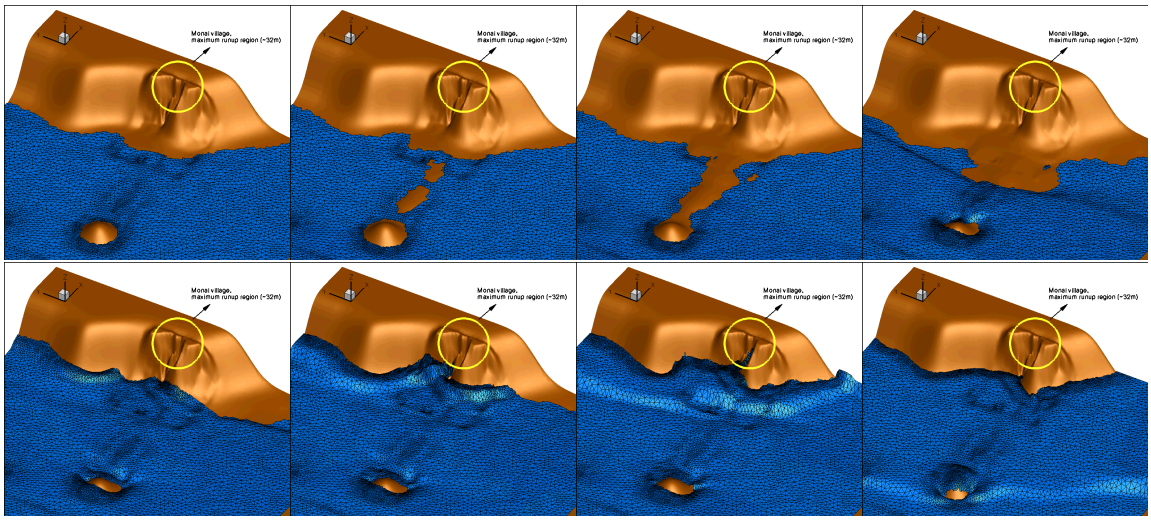

Figure 24: The Okushiri Tsunami experiment. From left to right, and from top to bottom : 3D visualization of the inundation and reflection process

During the experiment, probes have been set to measure the water height history in three locations shown in the top left picture on figure 25. On the same figure, we report the comparison of the computed water height deviation from it initial value, with the experimental data provided on the web page of the workshop. Two remarks can be made. Firstly, the agreement between measured and computed heights is quite satisfactory. Second, there is no remarkable difference between the results obtained on the coarse and fine mesh in the probes.

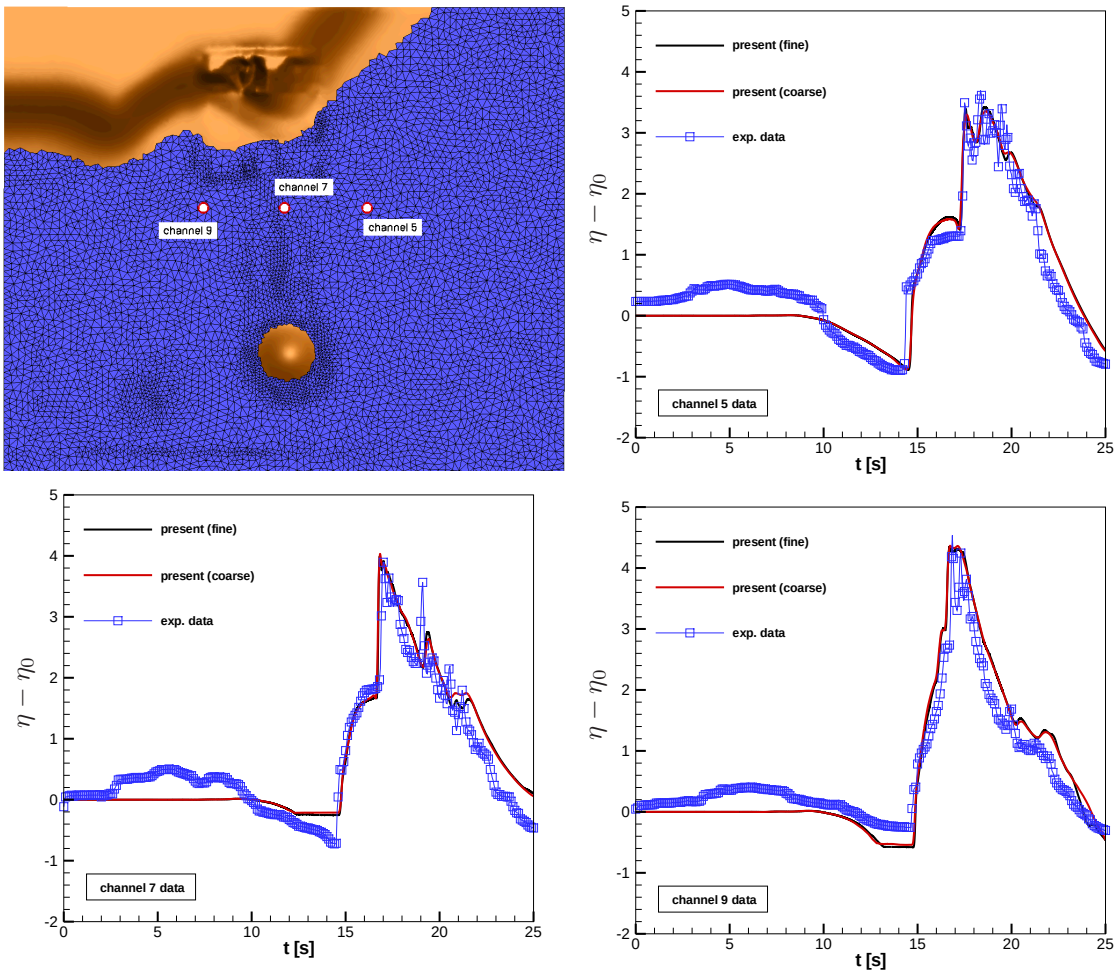

Figure 25: The Okushiri Tsunami experiment. Experimental gauges positions (top left) and comparisons with experiments in channels 5 (top right), 7 (bottom left) and 9 (bottom right)

As a last verification, we present on figure 26 the maximum runup plot obtained on the coarse and fine meshes. The plot has been obtained as described in section §5.3.2 for the conical island test. In the runup plots we have reported as a reference, the curve corresponding to the maximum experimental runup of 32 $[m]$ (real life scale). The pictures clearly show that the higher resolution allows to obtain a finer description of the runup region, especially in the steep area of the Monai village. In particular, the coarse mesh results underestimate the maximum runup by roughly 10 $[m]$, while the fine mesh results overshoot the line of the 32 $[m]$ by one row of giving a more conservative prediction of the maximum runup of about 36 meters.

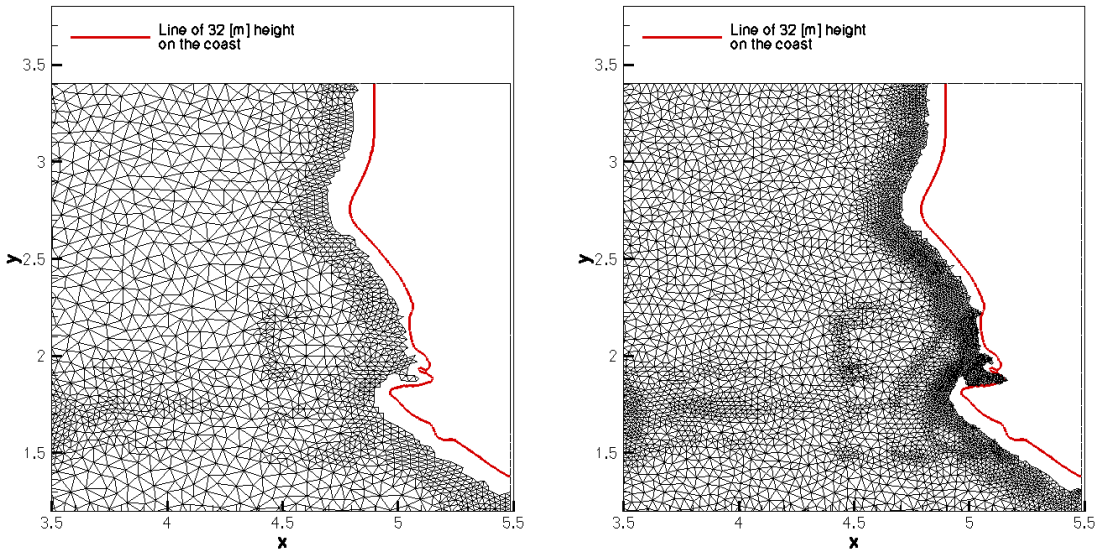

Figure 26: The Okushiri Tsunami experiment. Maximum run up plots on the coarse (left) and fine (right) mesh.

6 Conclusions

In this paper we have discussed a genuinely explicit residual discretization of the Shallow-Water equations based on an improved and adapted formulation of the nonlinear stabilized explicit limited Lax-Friedrich's scheme of [53]. The scheme has been shown to enjoy all the most interesting properties relevant for Shallow Water applications, namely the C-property and its generalization to moving equilibria, positivity preservation, and a robust handling of the wetting/drying front. As shown in the numerical results section, this work represents a considerable improvement over previous work by the author and his collaborators [54, 56, 55, 52], providing the same properties and similar accuracy with a much reduced computational cost. Theoretical results and thorough benchmarking have confirmed this fact. Following the initial work of [53], this paper finally brings Residual Distribution schemes to a cost similar to that of explicit second order Godunov type schemes (including DG), retaining all the advantages of the continuous residual based formulation.

The scheme has been already combined with uncertainty quantification techniques to study the sensitivity of long wave runup simulations to variations in physical parameters [57], and for robust code-to-code validation [22]. In this last reference, in particular, it has been shown that, in long wave runup simulations, the scheme proposed here provides accuracy levels very close to state of the art high order finite volume schemes.

Concerning the scheme, foreseen improvements are the design of higher (at least third) order formulations, and the use of ALE based moving mesh techniques for mesh adaptation, in particular to follow moving shorelines. Concerning the extension to other models, future work will involve the inclusion of Coriolis terms as already shown in [65], and eventually a formulation of the schemes on manifolds as in [63]. Current work also includes the investigation of residual based discretizations of non-hydrostatic models [60, 59].

A Proof of proposition 4.2

Proof of Lemma 4.1

To prove the lemma we start by noting that for $b \in H^{p+1}$ with $p \geq \min(p_f, p_v + 1) \geq 1$ we can write for exact integration (cf. equation (39))

$$\phi^K(v_0, b) = \oint_{\partial K} \boldsymbol{\mathcal{F}}(u(v_h, b)) \cdot \vec{n} + \int_K \boldsymbol{\mathcal{S}}(u(v_h, b), \nabla b) = \int_K \Big(\frac{\partial \boldsymbol{\mathcal{F}}}{\partial v}(v_0, b) \cdot \nabla v_0 + \mathcal{S}_v(v_0, \cdot \nabla b) + \boldsymbol{\mathcal{S}}(v_0, b, \nabla b) \Big)$$

Since v_0 is an invariant, and it describes a steady equilibrium, then we deduce immediately that (cf. (39) and (20))

$$\nabla v_0 = 0\,, \quad \mathcal{S}_v(v_0, \cdot \nabla b) + \boldsymbol{\mathcal{S}}(v_0, b, \nabla b) = 0$$

As a consequence, we deduce that $\phi^K(v_0, b) = 0$.

For the second part of the proof, due to the assumed regularity of $(v, b) \mapsto \boldsymbol{\mathcal{F}}(u(v, b))$, and since $v_h = v_0$ which is constant, then we deduce that $\boldsymbol{\mathcal{F}}_h = \boldsymbol{\mathcal{F}}(u(v_0, b))$ has the same regularity of b, which means that $\boldsymbol{\mathcal{F}}(u(v_0, b)) \in H^{p+1}(\Omega_h)$. Similarly, we argue that $\boldsymbol{\mathcal{S}}_h = \boldsymbol{\mathcal{S}}(u(v_0, b), \nabla b)$ is in H^p. We now consider on each K, the polynomials $\widehat{\boldsymbol{\mathcal{F}}}_h$ of degree p_f, and the polynomials $\widetilde{\boldsymbol{\mathcal{S}}}_h$ of degree p_v such that, denoting by f the generic face of ∂K (we omit the additional superscript ^{K})

$$\sum_{q=1}^{f_q} \omega_q \boldsymbol{\mathcal{F}}_h(\vec{x}_q) \cdot \vec{n}_f = \int_f \widehat{\boldsymbol{\mathcal{F}}}_h \cdot \vec{n}_f \quad \text{and} \quad \sum_{q=1}^{v_q} \overline{\omega}_q \boldsymbol{\mathcal{S}}_h(\vec{x}_q) = \int_K \widetilde{\boldsymbol{\mathcal{S}}}_h$$

With this notation, we can write, subtracting the exact integral which is zero :

$$\begin{aligned}
|\phi^K(v_0, b)| &= \Big| \sum_{f \in \partial K} \int_f \widehat{\boldsymbol{\mathcal{F}}}_h \cdot \vec{n}_f + \int_K \widetilde{\boldsymbol{\mathcal{S}}}_h \Big| \\
&= \Big| \sum_{f \in \partial K} \int_f (\widehat{\boldsymbol{\mathcal{F}}}_h - \boldsymbol{\mathcal{F}}(u(v_0, b))) \cdot \vec{n}_f + \int_K (\widetilde{\boldsymbol{\mathcal{S}}}_h - \boldsymbol{\mathcal{S}}(u(v_0, b), \nabla b)) \Big| \\
&\leq \sum_{f \in \partial K} \int_f \big| (\widehat{\boldsymbol{\mathcal{F}}}_h - \boldsymbol{\mathcal{F}}(u(v_0, b))) \cdot \vec{n}_f \big| + \int_K \big| \widetilde{\boldsymbol{\mathcal{S}}}_h - \boldsymbol{\mathcal{S}}(u(v_0, b), \nabla b) \big|
\end{aligned}$$

For the given regularity of b, we can write using standard approximation arguments [21, 28]

$$\big| \widehat{\boldsymbol{\mathcal{F}}}_h - \boldsymbol{\mathcal{F}}(u(v_0, b)) \big| \leq C(v_0, b)\, h^{p_f+1} \Rightarrow \int_f \big| (\widehat{\boldsymbol{\mathcal{F}}}_h - \boldsymbol{\mathcal{F}}(u(v_0, b))) \cdot \vec{n}_f \big| = \mathcal{O}(h^{p_f+2})$$

$$\big| \widetilde{\boldsymbol{\mathcal{S}}}_h - \boldsymbol{\mathcal{S}}(u(v_0, b), \nabla b) \big| \leq C'(v_0, b) h^{p_v+1} \Rightarrow \int_K \big| \widetilde{\boldsymbol{\mathcal{S}}}_h - \boldsymbol{\mathcal{S}}(u(v_0, b), \nabla b) \big| = \mathcal{O}(h^{p_v+3})$$

This leads to the final estimate $|\phi^K(v_0, b)| \leq C'' \max(h^{p_f+2}, h^{p_v+3})$.

Proof of Proposition 4.2

In order to prove the proposition, we rewrite the truncation error (32) or a steady smooth equilibrium $v = v_0$. First of all, the predictor step (33) provides an estimate on the error $\|w^* - u^0\|$, with

$u^0 = u(v_0, b)$. Indeed, from

$$|C_i|\frac{w_i^* - u_i^0}{\Delta t^n} + \sum_{K\in K_i} \beta_i^K \phi^K(v_0, b) = 0$$

and using Lemma 4.1 and (34) we immediately deduce that for exact integration $w^* = u^0$, and it is trivial to see that the (32) is identically zero due to Lemma 4.1.

For approximate integration we have, setting $u^0 = u(v_0, b)$

$$\|w_h^* - u^0\| = \mathcal{O}(h^l)\,, \quad l = \min(p_f + 1,\, p_v + 2) \tag{56}$$

Note that u_0 itself *is not constant*. We then write (recall that $w = u^0$)

$$\begin{aligned}|C_i|\frac{w_i^{n+1} - w_i^*}{\Delta t^n} + \sum_{K\in K_i} \Phi_i^K(w_h^n, w_h^*) &= |C_i|\frac{u_i^0 - w_i^*}{\Delta t^n} + \sum_{K\in K_i} \beta_i^K \left(\int_K \frac{w_h^* - u_h^0}{\Delta t^n} + \frac{1}{2}\phi^K(w_h^*) + \frac{1}{2}\phi^K(u^0) \right) \\ &= \sum_{K\in K_i} \beta_i^K \int_K \frac{w_h^* - u^0}{\Delta t^n} + \sum_{K\in K_i} \beta_i^K \phi^K(u_h^0) + \frac{1}{2}\sum_{K\in K_i} \beta_i^K \left(\phi^K(w_h^*) - \phi^K(u^0)\right)\end{aligned}$$

Note that here, consistently with the assumptions ofr the proposition, $\phi^K(w_h^*) = \phi^K(u(v_h^*, b))$. Now, following the the proof of lemma 4.1, we first introduce on each K the polynomials $\widehat{\boldsymbol{\mathcal{F}}}_h(u_h)$, of degree p_f, and $\widetilde{\boldsymbol{\mathcal{S}}}_h(u_h, \nabla b)$, of degree p_v, such that the numerical quadrature is equivalent to exact quadrature w.r.t these polynomials. Note that the dependence on u_h has been added for the following analysis. Next, if $\{\varphi_i\}_{i\in\Omega_h}$ we denote the P^1 finite element basis functions, following *e.g.* [54, 53, 50] we consider the Galerkin residuals

$$\phi_i^{\mathrm{G}}(u_h) = \int_K \varphi_i \big(\nabla\cdot\widehat{\boldsymbol{\mathcal{F}}}_h(u_h) + \widetilde{\boldsymbol{\mathcal{S}}}_h(u_h, \nabla b)\big)$$

Concerning the evaluation of these integrals the only constraint is that we have exactly

$$\sum_{j\in K} \phi_j^{\mathrm{G}}(u_h) = \int_K \left(\nabla\cdot\widehat{\boldsymbol{\mathcal{F}}}_h(u_h) + \widetilde{\boldsymbol{\mathcal{S}}}_h(u_h, \nabla b)\right) = \sum_{j\in K} \beta_j^K \phi^K(u_h)$$

which is always the case. Since these integrals do not appear in the actual discretization, we are allowed to assume that they are evaluated *exactly*. The exact evaluation implies that each $\phi_i^{\mathrm{G}}(u_h)$ is computed by means of quadrature formulae one degree more accurate than those used to compute $\phi^K(u_h)$. In particular, it implies that the quadrature is exact for both the p_f degree polynomial $\varphi_i\nabla\cdot\widehat{\boldsymbol{\mathcal{F}}}_h$, and for the $p_v + 1$ degree polynomial $\varphi_i\widetilde{\boldsymbol{\mathcal{S}}}_h$. This allows to gain one order of accuracy in the estimates. In particular, with arguments similar to those used in the proof of lemma 4.1, and using the regularity assumptions on ψ we can state that

$$\begin{aligned}\sum_{j\in K} \psi_j \int_K \varphi_j \nabla\cdot\widehat{\boldsymbol{\mathcal{F}}}_h(u_h) &= \int_K \psi_h \nabla\cdot\widehat{\boldsymbol{\mathcal{F}}}_h(u_h) = \int_K \psi\nabla\cdot\boldsymbol{\mathcal{F}}(u) + \mathcal{O}(h^{p_f+3}) \\ \sum_{j\in K} \psi_j \int_K \varphi_j \widetilde{\boldsymbol{\mathcal{S}}}_h(u_h, \nabla b) &= \int_K \psi_h \widetilde{\boldsymbol{\mathcal{S}}}_h(u_h, \nabla b) = \int_K \psi\boldsymbol{\mathcal{S}}(u, \nabla b) + \mathcal{O}(h^{p_v+4})\end{aligned} \tag{57}$$

Finally, we can easily recast the error (32) as (see for example [54, 53, 50])

$$\epsilon = \mathrm{I} + \mathrm{II} + \mathrm{III} + \mathrm{IV}$$

with

$$\mathrm{I} = \int_0^T \int_{\Omega_h} \psi_h (w_h^* - u_h^0) + \int_0^T \sum_{K\in\Omega_h} \int_K \psi_h \nabla\cdot \widehat{\boldsymbol{\mathcal{F}}}_h + \int_0^T \sum_{K\in\Omega_h} \int_K \widetilde{\boldsymbol{\mathcal{S}}}_h \psi_h$$

$$\mathrm{II} = \sum_{n=0}^N \frac{\Delta t^n}{2} \sum_{K\in\Omega_h} \int_K \psi_h \nabla\cdot (\widehat{\boldsymbol{\mathcal{F}}}_h(w_h^*) - \widehat{\boldsymbol{\mathcal{F}}}(u^0)) + \sum_{n=0}^N \frac{\Delta t^n}{2} \sum_{K\in\Omega_h} \int_K (\widetilde{\boldsymbol{\mathcal{S}}}_h(w_h^*, \nabla b) - \widetilde{\boldsymbol{\mathcal{S}}}(u^0, \nabla b))\psi_h$$

$$\begin{aligned}\mathrm{III} = &\sum_{n=0}^N \sum_{K\in\Omega_h} \sum_{i,j\in K} \frac{\psi_i - \psi_j}{3} \int_K (\beta_i^K - \varphi_i)(w_h^* - u_h^0) \\ &+ \sum_{n=0}^N \sum_{K\in\Omega_h} \sum_{i,j\in K} \Delta t^n \frac{\psi_i - \psi_j}{3} \int_K (\beta_i^K - \varphi_i) \nabla\cdot \widehat{\boldsymbol{\mathcal{F}}}_h(u^0) \\ &+ \sum_{n=0}^N \sum_{K\in\Omega_h} \sum_{i,j\in K} \Delta t^n \frac{\psi_i - \psi_j}{3} \int_K (\beta_i^K - \varphi_i) \widetilde{\boldsymbol{\mathcal{S}}}_h(u^0, \nabla b)\end{aligned}$$

$$\begin{aligned}\mathrm{IV} = &\sum_{n=0}^N \sum_{K\in\Omega_h} \sum_{i,j\in K} \frac{\Delta t^n}{2} \frac{\psi_i - \psi_j}{3} \int_K (\beta_i^K - \varphi_i) \nabla\cdot (\widehat{\boldsymbol{\mathcal{F}}}_h(w_h^*) - \widehat{\boldsymbol{\mathcal{F}}}_h(u^0)) \\ &+ \sum_{n=0}^N \sum_{K\in\Omega_h} \sum_{i,j\in K} \frac{\Delta t^n}{2} \frac{\psi_i - \psi_j}{3} \int_K (\beta_i^K - \varphi_i)(\widetilde{\boldsymbol{\mathcal{S}}}_h(w^*, \nabla b) - \widetilde{\boldsymbol{\mathcal{S}}}_h(u^0, \nabla b))\end{aligned}$$

We can now estimate each term using the results and hypotheses available. In particular, we will make use of (56), (57), (34), (37), and the regularity of ψ.

Term I, is easily estimated, considering that, being u^0 a smooth exact steady solution we can write

$$\begin{aligned}\mathrm{I} = \int_0^T \int_{\Omega_h} \psi_h (w_h^* - u_h^0) + \int_0^T \sum_{K\in\Omega_h} \int_K \Big(\psi_h \nabla\cdot \widehat{\boldsymbol{\mathcal{F}}}_h(u(v_0, b) - \psi \nabla\cdot \boldsymbol{\mathcal{F}}(u^0)\Big) \\ + \int_0^T \sum_{K\in\Omega_h} \int_K (\psi_h \widetilde{\boldsymbol{\mathcal{S}}}_h(u^0, \nabla b) - \psi \boldsymbol{\mathcal{S}}(u(v_0, b), \nabla b))\end{aligned}$$

Using now (56), (57), and the fact that if (34) is true, then the number of triangles in a two dimensional grid is of $\mathcal{O}(h^{-2})$, we immediately deduce

$$|\mathrm{I}| \leq C(\Omega_h, T)\, h^l \tag{58}$$

A similar argument can be used to estimate the term III. In particular, we can again use the fact

that $\nabla\cdot\boldsymbol{\mathcal{F}}(u^0)+\boldsymbol{\mathcal{S}}(u^0,\nabla b)=0$ to recast this term as

$$\begin{aligned}
\text{III} =& \sum_{n=0}^{N}\sum_{K\in\Omega_h}\sum_{i,j\in K}\frac{\psi_i-\psi_j}{3}\int_K(\beta_i^K-\varphi_i)(w_h^*-u_h^0)\\
&+\sum_{n=0}^{N}\sum_{K\in\Omega_h}\sum_{i,j\in K}\Delta t^n\frac{\psi_i-\psi_j}{3}\int_K(\beta_i^K-\varphi_i)\nabla\cdot\left(\widehat{\boldsymbol{\mathcal{F}}}_h(u^0)-\boldsymbol{\mathcal{F}}(u^0)\right)\\
&+\sum_{n=0}^{N}\sum_{K\in\Omega_h}\sum_{i,j\in K}\Delta t^n\frac{\psi_i-\psi_j}{3}\int_K(\beta_i^K-\varphi_i)\left(\widetilde{\boldsymbol{\mathcal{S}}}_h(u^0,\nabla b)-\boldsymbol{\mathcal{S}}(u^0,\nabla b)\right)
\end{aligned}$$

For a smooth solution, provided that (34) holds we can initially write

$$\begin{aligned}
|\text{III}| \leq& C_T\Delta t^{-1}C_{\Omega_h}h^{-2}\frac{h}{3}\|\nabla\psi\|_{L^\infty}C_Kh^2(1+\sup_{\substack{K\in\Omega_h\\ i\in K}}\|\beta_i^K\|_K)\|w_h^*-u_h^0\|_K\\
&+C_TC_{\Omega_h}h^{-2}\frac{h}{3}\|\nabla\psi\|_{L^\infty}C_Kh^2(1+\sup_{\substack{K\in\Omega_h\\ i\in K}}\|\beta_i^K\|_K)\|\nabla\cdot\left(\widehat{\boldsymbol{\mathcal{F}}}_h(u^0)-\boldsymbol{\mathcal{F}}(u^0)\right)\|_K\\
&+C_TC_{\Omega_h}h^{-2}\frac{h}{3}\|\nabla\psi\|_{L^\infty}C_Kh^2(1+\sup_{\substack{K\in\Omega_h\\ i\in K}}\|\beta_i^K\|_K)\|\widetilde{\boldsymbol{\mathcal{S}}}_h(u^0,\nabla b)-\boldsymbol{\mathcal{S}}(u^0,\nabla b)\|_K
\end{aligned}$$

and using (34) plus standard arguments to estimate the approximation error of the polynomials $\widehat{\boldsymbol{\mathcal{F}}}$ of degree p_f and $\widetilde{\boldsymbol{\mathcal{S}}}$ of degree p_v [21, 28], we end with

$$\begin{aligned}
|\text{III}| \leq& \sup_{K\in\Omega_h}\left(C_\alpha\|w_h^*-u_h^0\|_K+C_\beta h\|\nabla\cdot\left(\widehat{\boldsymbol{\mathcal{F}}}_h(u^0)-\boldsymbol{\mathcal{F}}(u^0)\right)\|_K+C_\gamma h\|\widetilde{\boldsymbol{\mathcal{S}}}_h(u^0,\nabla b)-\boldsymbol{\mathcal{S}}(u^0,\nabla b)\|_K\right)\\
\leq& C'_\alpha h^l+C'_\beta h^{p_f+1}+C'_\gamma h^{p_v+2}\leq(C'_\alpha+C'_\beta+C'_\gamma)h^l=\mathcal{O}(h^l)
\end{aligned}\tag{59}$$

To end the proof we need to estimate II and IV. To to this, we use the hypothesis on the Lipschitz continuity of the flux and source (37). In particular, first, using the edge continuity of the flux approximation, we recast II as

$$\text{II}=-\sum_{n=0}^{N}\frac{\Delta t^n}{2}\sum_{K\in\Omega_h}\int_K(\widehat{\boldsymbol{\mathcal{F}}}_h(w_h^*)-\widehat{\boldsymbol{\mathcal{F}}}(u^0))\cdot\nabla\psi_h+\sum_{n=0}^{N}\frac{\Delta t^n}{2}\sum_{K\in\Omega_h}\int_K(\widetilde{\boldsymbol{\mathcal{S}}}_h(w_h^*,\nabla b)-\widetilde{\boldsymbol{\mathcal{S}}}(u^0,\nabla b))\psi_h$$

We next use (37) to obtain

$$\|\widehat{\boldsymbol{\mathcal{F}}}_h(w_h^*)-\widehat{\boldsymbol{\mathcal{F}}}_h(u^0)\|_K\leq\mathcal{K}_{\boldsymbol{\mathcal{F}}}\|w_h^*-u^0\|_K\leq C_Kh^l\,,\ \|\widetilde{\boldsymbol{\mathcal{S}}}_h(w_h^*,\nabla b)-\widetilde{\boldsymbol{\mathcal{S}}}_h(u^0,\nabla b)\|\leq\mathcal{K}_{\boldsymbol{\mathcal{S}}}\|w_h^*-u^0\|\leq C'_Kh^l$$

and, thus we can bound this term as

$$|\text{II}|\leq C_{\Omega_h}h^{-2}h^2(\|\nabla\psi\|_{L^\infty}C_K+\|\psi\|_\infty C'_K)h^l=\mathcal{O}(h^l)\tag{60}$$

The last term is estimated in a similar way. In particular, we first rewrite the polynomial $\widehat{\boldsymbol{\mathcal{F}}}_h$ as a high order approximation

$$\widehat{\boldsymbol{\mathcal{F}}}_h=\sum_\sigma\boldsymbol{\mathcal{F}}_\sigma\widehat{\varphi}_\sigma$$

with the $\widehat{\varphi}_\sigma$the kernel of a higher degree (at least p_f) Lagrange approximation. Next we observe that

$$\|\nabla\cdot(\widehat{\boldsymbol{\mathcal{F}}}_h(w*)-\widehat{\boldsymbol{\mathcal{F}}}_h(u^0))\|_K = \|\sum_\sigma(\boldsymbol{\mathcal{F}}(w^*_\sigma)-\boldsymbol{\mathcal{F}}(u^0_\sigma))\cdot\nabla\widehat{\varphi}_\sigma\|_K \leq \widehat{C}_K h^{-1}\mathcal{K}_{\boldsymbol{\mathcal{F}}}\sum_\sigma\|w^*_\sigma-u^0_\sigma\| \leq \widehat{C}'_K h^{l-1}$$

Finally, the term IV can be estimated as (cf. (37) and (56))

$$\begin{aligned}|\mathrm{IV}| \leq & C_{\Omega_h}h^{-2}\|\nabla\psi\|_{L^\infty}h\,h^2(1+\sup_{\substack{K\in\Omega_h\\ i\in K}}\|\beta_i^K\|_K)\widehat{C}'_K h^{l-1}\\ &+C_{\Omega_h}h^{-2}\|\nabla\psi\|_{L^\infty}h\,h^2(1+\sup_{\substack{K\in\Omega_h\\ i\in K}}\|\beta_i^K\|_K)\mathcal{K}_{\boldsymbol{\mathcal{S}}}\widetilde{C}_K h^l \leq C(\Omega_h,\|\nabla\psi\|_{L^\infty},\mathcal{K}_{\boldsymbol{\mathcal{F}}},\mathcal{K}_{\boldsymbol{\mathcal{S}}})h^l\end{aligned} \tag{61}$$

which together with (58), (60), and (59) achieves the proof.

B Proof of proposition 4.7

To prove proposition 4.7 we use the properties of the limiter and the definition of the LF distribution recalled in section §4.3, in particular (47) (see [53, 56] for more details), The explicit limited Lax-Friedrich's (LLF) scheme obtained by applying the limiter equation by equation leads to the following updates for the water height

1. First step
$$|C_i|(H_i^1-H_i^n) = -\Delta t\sum_{T|i\in T}\gamma_i\sum_{j\neq i,\,j\in T}\frac{1}{3}\Big(\alpha_{\mathrm{LF}}-k_j^n\Big)(H_i^n-H_j^n)$$

2. Second step
$$\begin{aligned}|C_i|(H_i^{n+1}-H_i^1) = -\Delta t\sum_{T|i\in T}\gamma_i\Big(&\frac{|T|}{3}\frac{H_i^1-H_i^n}{\Delta t}+\sum_{j\neq i,\,j\in T}\frac{1}{6}\big(\alpha_{\mathrm{LF}}-k_j^n\big)(H_i^n-H_j^n)\\ &+\sum_{j\neq i,\,j\in T}\frac{1}{6}\big(\alpha_{\mathrm{LF}}-k_j^1\big)(H_i^1-H_j^1)\Big)\end{aligned}$$

where

$$k_j=\frac{\vec{u}_j\cdot\vec{n}_j}{2}$$

with $\vec{n}_j$ the inward normal to the edge facing node j, scaled by its length l_j. By definition of α_{LF}, $\alpha_{\mathrm{Lf}}-k_j\geq 0$ (cf. equations (45) and (47), and section §4.5). If $H_i^n\geq 0,\ \forall i$, the positivity of H_i^1 is easily shown to lead to the condition

$$\Delta t\frac{\gamma_i}{3}(2\alpha_{\mathrm{LF}}+k_i^n)\leq|C_i|$$

which, using the fact that $\gamma_i^n\geq 0$ and $\alpha_{\mathrm{LF}}\geq k_j$ (cf. equations (45) and (47), section §4.5 and see [56]), can be replaced by the stricter constraint in the first slot of the $\min(\cdot,\cdot)$ operator in (48). The second iteration can be recast as

$$\begin{aligned}|C_i|H_i^{n+1} = &\sum_{T|i\in T}(1-\gamma_i)\frac{|T|}{3}H_i^1-\frac{\Delta t}{2}\sum_{T|i\in T}\gamma_i\frac{2\alpha_{\mathrm{LF}}+k_i}{3}H_i^1+\sum_{T|i\in T}\gamma_i\Big(\frac{|T|}{3}-\frac{\Delta t}{2}\frac{2\alpha_{\mathrm{LF}}+k_i}{3}\Big)H_i^n\\ &+\frac{\Delta t}{2}\sum_{T|i\in T}\gamma_i\sum_{j\neq i}\frac{\alpha_{\mathrm{LF}}-k_j}{3}H_j^1+\frac{\Delta t}{2}\sum_{T|i\in T}\gamma_i\sum_{j\neq i}\frac{\alpha_{\mathrm{LF}}-k_j}{3}H_j^n\end{aligned}$$

Setting

$$\omega_i = \sum_{T|i\in T} \gamma_i \frac{2\alpha_{\rm LF}+k_i}{3} \, ,$$

adding and substracting H_i^n in the second term on the right hand side, and using the first iteration, we can recast the last expression as

$$\begin{aligned}
C_i|H_i^{n+1} &= \sum_{T|i\in T}(1-\gamma_i)\frac{|T|}{3}H_i^1 + \sum_{T|i\in T}\gamma_i\Big(\frac{|T|}{3}-\Delta t\frac{2\alpha_{\rm LF}+k_i}{3}\Big)H_i^n + \frac{\Delta t^2}{2}\frac{\omega_i}{|C_i|}\sum_{T|i\in T}\gamma_i\sum_{j\neq i}\frac{\alpha_{\rm LF}-k_j}{3}(H_i^n-H_j^n) \\
&+ \frac{\Delta t}{2}\sum_{T|i\in T}\gamma_i\sum_{j\neq i}\frac{\alpha_{\rm LF}-k_j}{3}H_j^1 + \frac{\Delta t}{2}\sum_{T|i\in T}\gamma_i\sum_{j\neq i}\frac{\alpha_{\rm LF}-k_j}{3}H_j^n \\
&= \sum_{T|i\in T}(1-\gamma_i)\frac{|T|}{3}H_i^1 + \sum_{T|i\in T}\gamma_i\Big(\frac{|T|}{3}-\Delta t\frac{2\alpha_{\rm LF}+k_i}{3}+\frac{\Delta t^2}{2}\frac{\omega_i}{|C_i|}\frac{2\alpha_{\rm LF}+k_i}{3}\Big)H_i^n \\
&+ \frac{\Delta t}{2}\sum_{T|i\in T}\gamma_i\sum_{j\neq i}\frac{\alpha_{\rm LF}-k_j}{3}H_j^1 + \frac{\Delta t}{2}\sum_{T|i\in T}\sum_{j\neq i}\gamma_i\frac{\alpha_{\rm LF}-k_j}{3}\left(1-\frac{\Delta t\omega_i}{|C_i|}\right)H_j^n
\end{aligned}$$

Due to the definition of ω_i, the result is non-negative as long as $H_j^n \geq 0\,, \forall\, j$, and as long as (48) is verified.

Acknowledgements

The adaptive meshes used in this paper have been produced with the MMG3D software (see `http://www.math.u-bordeaux1.fr/~cdobrzyn/logiciels/mmg3d.php`) which is developed and maintained by Cécile Dobrzynski, who the author warmly thanks.

References

[1] R. Abgrall. Essentially non oscillatory residual distribution schemes for hyperbolic problems. *J. Comput. Phys*, 214(2):773–808, 2006.

[2] R. Abgrall. Residual distribution schemes: Current status and future trends. *Computers and Fluids*, 35(7):641 – 669, 2006.

[3] R. Abgrall. A review of residual distribution schemes for hyperbolic and parabolic problems: The july 2010 state of the art. *Comm.Comput.Phys.*, 11(4):1043–1080, 2012.

[4] R. Abgrall and T.J. Barth. Residual distribution schemes for conservation laws via adaptive quadrature. *SIAM J. Sci. Comput.*, 24(3):732–769, 2002.

[5] R. Abgrall, K. Mer, and B. Nkonga. A Lax–Wendroff type theorem for residual schemes. In M. Haffez and J.J. Chattot, editors, *Innovative methods for numerical solutions of partial differential equations*, pages 243–266. World Scientific, 2002.

[6] R. Abgrall and M. Mezine. Construction of second-order accurate monotone and stable residual distribution schemes for steady flow problems. *J. Comput. Phys.*, 195:474–507, 2004.

[7] R. Abgrall and P.L. Roe. High-order fluctuation schemes on triangular meshes. *J. Sci. Comput.*, 19(3):3–36, 2003.

[8] R. Abgrall and J. Trefilik. An example of high order residual distribution scheme using non-lagrange elements. *Journal of Scientific Computing*, 45:3–25, 2010.

[9] E. Audusse and M.-O. Bristeau. A well-balanced positivity preserving second-order scheme for shallow water flows on unstructured meshes. *Journal of Computational Physics*, 206(1):311 – 333, 2005.

[10] T.J. Barth. Numerical methods for conservation laws on structured and unstructured meshes. *VKI LS 2003-05, 33rd Computational Fluid dynamics Course, von Karman Institute for Fluid Dynamics*, 2003.

[11] A. Bermudez and M.E. Vazquez. Upwind methods for hyperbolic conservation laws with source terms. *Computers & Fluids*, 23(8):1049 – 1071, 1994.

[12] P. Bonneton, E. Barthelemy, F. Chazel, R. Cienfuegos, D. Lannes, F. Marche, and M. Tissier. Recent advances in serre-green naghdi modelling for wave transformation, breaking and runup processes. *European Journal of Mechanics - B/Fluids*, In Press, Corrected Proof:–, 2011.

[13] M.J. Briggs, C.E. Synolakis, G.S. Harkins, and D.R. Green. Laboratory experiments of tsunami runup on a circular island. *Pure and Applied Geophysics*, 144:569–593, 1995.

[14] P. Brufau and P. Garcia-Navarro. Unsteady free surface flow simulation over complex topography with a multidimensional upwind technique. *Journal of Computational Physics*, 186(2):503 – 526, 2003.

[15] P. Brufau, P. Garcia-Navarro, and M.E. Vazquez-Cendon. Zero mass error using unsteady wetting-drying conditions in shallow flows over dry irregular topography. *Int. J. Numer. Meth. Fluids*, 45:1047–1082, 2004.

[16] P. Brufau, M.E. Vazquez-Cendon, and P. Garcia-Navarro. A numerical model for the flooding and drying of irregular domains. *Int. J. Numer. Meth. Fluids*, 39:247–275, 2002.

[17] V. Caleffi, A. Valliani, and A. Zanni. Finite volume method for simulating extreme flood events in natural channels. *J.of Hydraulic Research*, 41(2):167–177, 2003.

[18] M.J. Castro, A.M. Ferreiro Ferreiro, J.A. Garcia-Rodriguez, J.M. Gonzalez-Vida, J. Macias, C. Pares, and M.E. Vazquez-Cendon. The numerical treatment of wet/dry fronts in shallow flows: application to one-layer and two-layer systems. *Mathematical and Computer Modelling*, 42(3-4):419 – 439, 2005.

[19] M.J. Castro, J. Gonzalez-Vida, and C. Pares. Numerical treatment of wet/dry fronts in shallow flows with a roe scheme. *Mathematical Models and Methods in Applied Sciences*, 16(6):897–931, 2006.

[20] L. Cea and M.E. Vazquez-Cendon. Unstructured finite volume discretization of bed friction and convective flux in solute transport models linked to the shallow water equations. *J.Comput.Phys.*, 231(8):3317–3339, 2011.

[21] P.G. Ciarlet and P.A. Raviart. General lagrange and hermite interpolation in $\mathbb{R}^n$ with applications to finite element methods. *Arch.Ration.Mech.Anal.*, 46:177–199, 1972.

[22] P.M. Congedo, A.I. Delis, and M. Ricchiuto. Robust code-to-code comparison for long wave run up. SIAM Conf. on Mathematical and Computational Issues in the Geosciences, Padova (Italy), June 2013.

[23] Á. Csík, M. Ricchiuto, and H. Deconinck. A conservative formulation of the multidimensional upwind residual distribution schemes for general nonlinear conservation laws. *J. Comput. Phys*, 179(2):286–312, 2002.

[24] H. Deconinck and M. Ricchiuto. Residual distribution schemes: foundation and analysis. In E. Stein, R. de Borst, and T.J.R. Hughes, editors, *Encyclopedia of Computational Mechanics*. John Wiley & Sons, Ltd., 2007. DOI: 10.1002/0470091355.ecm054.

[25] A.I. Delis, M.Kazolea, and N.A.Kampanis. A robust high-resolution finite volume scheme for the simulation of long waves over complex domains. *Int. J. for Numerical Methods in Fluids*, 56:419–452, 2008.

[26] A.I. Delis and N.Katsaounis. Relaxation schemes for the shallow water equations. *Int. J. for Numerical Methods in Fluids*, 41:695–719, 2003.

[27] D.A. Dunavant. High degree efficient symmetrical gaussian quadrature rules for the triangle. *Int. J. Numer. Methods in Engrg.*, 21:1129–1148, 1985.

[28] A. Ern and J.-C. Guermond. *Theory and practice of finite elements*, volume 159 of *Applied Mathematical Sciences*. Springer, 2004.

[29] A. Ern, S. Piperno, and K. Djadel. A well-balanced runge–kutta discontinuous galerkin method for the shallow-water equations with flooding and drying. *Int. J. for Numerical Methods in Fluids*, 58(1):1–25, 2008.

[30] T. Gallouët, J.-M. Hérard, and N. Seguin. Some approximate godunov schemes to compute shallow-water equations with topography. *Computers & Fluids*, 32(4):479–513, 2003.

[31] P. Garcia-Navarro, J. Burguete, and R. Aliod. Numerical simulation of runoff over dry beds. *Monografias del Semin. Matem. Garcia de Galdeano*, 27:307–314, 2003.

[32] J.-F. Gerbeau and B. Perthame. Derivation of viscous saint-venant system for laminar shallow water ; numerical validation. *Discrete and Continuous Dynamical Systems, Ser. B*, 1(1):89–102, 2001.

[33] J.M. Greenberg and A.Y. Leroux. A well-balanced scheme for the numerical processing of source terms in hyperbolic equations. *SIAM J. Numer. Anal.*, 33:1–16, 1996.

[34] A. Harten. On the symmetric form of systems of conservation laws with entropy. *J. Comput. Phys.*, 49:151–164, 1983.

[35] G. Hauke. A symmetric formulation for computing transient shallow water flows. *Computer Methods in Applied Mechanics and Engineering*, 163(1-4):111–122, 1998.

[36] G. Hauke, A. Landaberea, I. Garmendia, and J. Canales. On the thermodynamics, stability and hierarchy of entropy functions in fluid flow. *Computer Methods in Applied Mechanics and Engineering*, 195(33-36):4473–4489, 2006.

[37] M. Hubbard and N. Dodd. A 2d numerical model of wave run-up and overtopping. *Coastal Engineering*, 47(1):1–26, 2002.

[38] M. Hubbard and P. Garcia-Navarro. Flux difference splitting and the balancing of source terms and flux gradients. *J. Comp. Phys.*, 165(1):89–125, 2000.

[39] M. Hubbard and M. Ricchiuto. Discontinuous upwind residual distribution: A route to unconditional positivity and high order accuracy. *Computers and Fluids*, 46(1):263 – 269, 2011.

[40] T.J.R. Hughes, G. Scovazzi, and T. Tezduyar. Stabilized methods for compressible flows. *J. Sci. Comp.*, 43:343–368, 2010.

[41] D. Lannes and P. Bonneton. Derivation of asymptotic two-dimensional time-dependent equations for surface water wave propagation. *Physics of Fluids*, 21, 2009. 016601 doi:10.1063/1.3053183.

[42] R.J. LeVeque. Balancing source terms and flux gradients in high-resolution godunov methods: the quasi-steady wave-propagation algorithm. *J. Comput. Phys.*, 146(1):346–365, 1998.

[43] P. L.-F. Liu, H. Yeh, and C. Synolakis, editors. *Advanced Numerical Models for Simulating Tsunami Waves and Runup*, volume 10 of *Advances in Coastal and Ocean Engineering*. World Scientific, 2008.

[44] F. Marche. Derivation of a new two-dimensional viscous shallow water model with varying topography, bottom friction and capillary effects. *European Journal of Mechanics - B/Fluids*, 26(1):49 – 63, 2007.

[45] I.K. Nikolos and A.I. Delis. An unstructured node-centered finite volume scheme for shallow water flows with wet/dry fronts over complex topography. *Computer Methods in Applied Mechanics and Engineering*, 198(47-48):3723 – 3750, 2009.

[46] S. Noelle, N. Pankratz, G. Puppo, and J.R. Natvig. Well-balanced finite volume schemes of arbitrary order of accuracy for shallow water flows. *J. Comput. Phys.*, 213(2):474–499, 2006.

[47] S. Noelle, Y. Xing, and C.-W. Shu. High order well-balanced finite volume weno schemes for shallow water equation with moving water. *J.Comput.Phys*, 226:29–58, 2007.

[48] S. Noelle, Y. Xing, and C.-W. Shu. High order well-balanced schemes. 2009.

[49] B. Perthame and C.-W. Shu. On positivity-preserving finite-volume schemes for euler equations. *Numerische Mathematik*, 73(1):119–130, 1996.

[50] M. Ricchiuto. *Contributions to the development of residual discretizations for hyperbolic conservation laws with application to shallow water flows*. Hdr, Université Sciences et Technologies - Bordeaux I, December 2011.

[51] M. Ricchiuto. Explicit Residual Discretizations for Shallow Water Flows. *Aip Conference Proceedings*, 1389(1):919–922, 2011.

[52] M. Ricchiuto. On the c-property and generalized c-property of residual distribution for the shallow water equations. *Journal of Scientific Computing*, 48:304–318, 2011.

[53] M. Ricchiuto and R. Abgrall. Explicit runge-kutta residual distribution schemes for time dependent problems: Second order case. *Journal of Computational Physics*, 229(16):5653 – 5691, 2010.

[54] M. Ricchiuto, R. Abgrall, and H. Deconinck. Application of conservative residual distribution schemes to the solution of the shallow water equations on unstructured meshes,. *J. Comput. Phys.*, 222:287–331, 2007.

[55] M. Ricchiuto and A. Bollermann. Accuracy of stabilized residual distribution for shallow water flows including dry beds. In E.Tadmor, J.G.Liu, and A.Tzavaras, editors, *HYP08: 12th international conference on hyperbolic problems : theory, numerics, applications*, volume 67(2). AMS, American Mathematical Society, 2009.

[56] M. Ricchiuto and A. Bollermann. Stabilized residual distribution for shallow water simulations. *J. Comput. Phys*, 228(4):1071–1115, 2009.

[57] M. Ricchiuto, P.M. Congedo, G. Geraci, and R. Abgrall. Uncertainty propagation in shallow water long wave run up simulations. First International Conference on Frontiers of Comput. Physics: Modelling the Earth System, Boulder (CO), USA, December 2012.

[58] M. Ricchiuto, Á. Csík, and H. Deconinck. Residual distribution for general time dependent conservation laws. *J. Comput. Phys*, 209(1):249–289, 2005.

[59] M. Ricchiuto and A.G. Filippini. Upwind Residual discretization of enhanced Boussinesq equations for wave propagation over complex bathymetries. Research Report RR-8311, INRIA, May 2013.

[60] M. Ricchiuto and A.G. Filippini. Upwind residual discretizations of the enhanced boussinesq equations for wave propagation over complex bathymetries. SIAM Conf. on Mathematical and Computational Issues in the Geosciences, Padova (Italy), June 2013.

[61] P.L. Roe. Fluctuations and signals - a framework for numerical evolution problems. In K.W. Morton and M.J. Baines, editors, *Numerical Methods for Fluids Dynamics*, pages 219–257. Academic Press, 1982.

[62] P.L. Roe. Computational fluid dynamics¿retrospective and prospective. *International Journal of Computational Fluid Dynamics*, 19(8):581–594, 2005.

[63] J.A. Rossmanith. Residual distribution schemes for hyperbolic balance laws in generalized coordinates. *Numerical Modeling of Space Plasma Flows, ASP Conference Series*, 359:213–219, 2006.

[64] D. Sarmany, M. Hubbard, and M. Ricchiuto. Unconditionally stable space-time discontinuous residual distribution for shallow-water flows. Research Report RR-7958, INRIA, 2012.

[65] D. Sarmany and M.E. Hubbard. Upwind residual distribution for shallow-water ocean modelling. *Ocean Modelling*, 64(0):1–11, 2013.

[66] M. Seaid. Non-oscillatory relaxation methods for the shallow water equations in one and two space dimensions. *Int. J. for Numerical Methods in Fluids*, 46:457–484, 2004.

[67] M. Seaïd. Non-oscillatory relaxation methods for the shallow-water equations in one and two space dimensions. *International Journal for Numerical Methods in Fluids*, 46(5):457–484, 2004.

[68] S.P. Spekreijse. Multigrid solution of monotone second-order discretizations of hyperbolic conservation laws. *Math. Comp.*, 49:135–155, 1987.

[69] C.E. Synolakis, E. Bernard, V. Titov, U. Kanoglu, and F. Gonzalez. Validation and verification of tsunami numerical models. *Pure and Applied Geophysics*, 165:2197–2228, 2008.

[70] J. Szmelter and P.K. Smolarkiewicz. An edge-based unstructured mesh discretisation in geospherical framework. *Journal of Computational Physics*, 229(13):4980 – 4995, 2010.

[71] J. Szmelter and P.K. Smolarkiewicz. An edge-based unstructured mesh framework for atmospheric flows. *Computers & Fluids*, 46(1):455 – 460, 2011.

[72] E. Tadmor. Skew-selfadjoint form for systems of conservation laws. *J. Math. Anal. Appl.*, 103:428–442, 1984.

[73] E. Tadmor. Skew-selfadjoint form for systems of conservation laws. *J. Math. Anal. Appl.*, 103:428–442, 1984.

[74] E. Tadmor. Entropy functions for symmetric systems of conservation laws. *J. Math. Anal. Appl.*, 122:355–359, 1987.

[75] E. Tadmor. Entropy functions for symmetric systems of conservation laws. *J. Math. Anal. Appl.*, 122:355–359, 1987.

[76] W.C. Thacker. Some exact solutions to the nonlinear shallow-water wave equations. *J. Fluid Mechanics*, 107:499–508, 1981.

[77] Y. Xing and C.-W. Shu. High-order well-balanced finite volume WENO schemes and discontinuous Galerkin methods for a class of hyperbolic systems with source terms. *J. Comput. Phys.*, 214(2):567–598, 2006.

[78] Y. Xing and C.-W. Shu. High-order finite volume weno schemes for the shallow water equations with dry states. *Advances in Water Resources*, 34(8):1026 – 1038, 2011.

[79] Y. Xing, C.-W. Shu, and S. Noelle. On the advantage of well-balanced schemes for moving-water equilibria of the shallow water equations. *Journal of Scientific Computing*, 48:339–349, 2011.

[80] Y. Xing, X. Zhang, and C.-W. Shu. Positivity-preserving high order well-balanced discontinuous galerkin methods for the shallow water equations. *Advances in Water Resources*, 33(12):1476 – 1493, 2010.

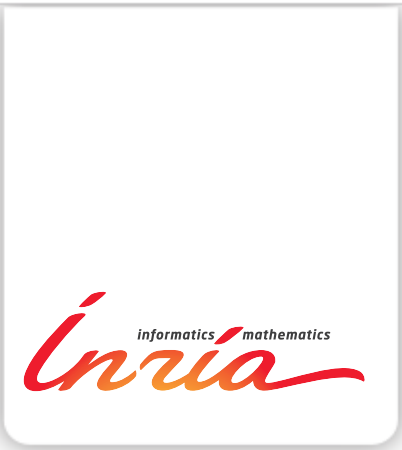

RESEARCH CENTRE
BORDEAUX – SUD-OUEST

351, Cours de la Libération
Bâtiment A 29
33405 Talence Cedex

Publisher
Inria
Domaine de Voluceau - Rocquencourt
BP 105 - 78153 Le Chesnay Cedex
inria.fr

ISSN 0249-6399